Conceptual models of dissolved carbon fluxes considering interannual typhoon responses under extreme climates in a two-layer stratified lake

Hao-Chi Lin[1], Keisuke Nakayama[2], Jeng-Wei Tsai[3], and Chih-Yu Chiu[4]

[1] Department of Geography, National Taiwan University, Taipei City, Taiwan
[2] Graduate School of Engineering, Kobe University, Kobe City, Japan
[3] Graduate Institute of Bioresources, National Pingtung University of Science and Technology, Pingtung, Taiwan
[4] Biodiversity Research Center, Academia Sinica, Taipei City, Taiwan

* Corresponding author: Keisuke Nakayama (nakayama@phoenix.kobe-u.ac.jp)

Abstract

Extreme climates affect the seasonal and interannual patterns of carbon (C) distribution due to the regimes of river inflow and thermal stratification within lentic ecosystems. Typhoons rapidly load substantial amounts of terrestrial C into small subtropical lakes (i.e., Yuan-Yang Lake, YYL), renewing and mixing the water column. We developed conceptual dissolved C model and hypothesized that allochthonous C loading and river inflow intrusion may affect the dissolved inorganic C (DIC) and dissolved organic C (DOC) distributions in a small subtropical lake under these extreme climates. A two-layer conceptual C models was developed to explore how the DIC and DOC fluxes respond to typhoon disturbances on seasonal and interannual time scales in YYL while simultaneously considering autochthonous processes such as algal photosynthesis, remineralization, and vertical transportation. Monthly field samplings were conducted to measure the DIC, DOC, and chlorophyll *a* concentrations to compare the temporal patterns of fluxes between typhoon years (2015–2016) and non-typhoon years (2017–2018). The results demonstrated that net ecosystem production was 3.14 times higher in the typhoon years than in the non-typhoon years in YYL. The results suggested that a load of allochthonous C was the most crucial factor affecting the temporal variation of C fluxes in the typhoon years because of changes in the physical and biochemical processes, such as photosynthesis, mineralization, and vertical transportation. However, the lowered vertical transportation rate shaped the seasonal C in the non-typhoon years due to thermal stratification within this small subtropical lake.

1. Introduction

The Intergovernmental Panel for Environmental Changes Sixth Assessment Report (IPCC AR6) (2021) suggested that, by 2050, not only is air temperature going to increase by at least about 1.5°C but high-intensity storms and drought events will become more frequent as a result of global warming and climate change. In freshwater ecosystems, extreme climates may change the mixing regimes of water columns (Kraemer et al., 2021; Maberly et al., 2020; Woolway et al., 2020), heat wave events (Woolway et al., 2021a; Woolway et al., 2021b), droughts (Marcé et al., 2019), and floods (Woolway et al., 2018). Freshwater ecosystems store around 0.32 to 1.8 Pg C yr^{-1}, which is approximately equivalent to shallow coastal areas; these ecosystems provide important services for human sustainability, such as acting as processing hotspots in regional carbon (C) cycling (Aufdenkampe et al., 2011; Cole et al., 2007; Engel et al., 2018; Lauerwald et al., 2015; Raymond et al., 2013). Extreme weather events might induce stronger seasonal thermal stratification from spring to summer and longer overturns from autumn to winter, thereby changing C distribution and transportation within water bodies (Kraemer et al., 2021; Olsson et al., 2022a; Woolway et al., 2020). The responses of C fluxes in small lakes (lake area < 1 km^2) are sensitive to climate change due to the ease with which C mixes with water columns (Doubek et al., 2021; MacIntyre et al., 2021; Winslow et al., 2015). Moreover, storms induce dramatic changes in thermal stratification and water inflows (Lin et al., 2022; Olsson et al., 2022b; Vachon and Del Giorgio, 2014; Woolway et al., 2018). River inflows and wind turbulence mix allochthonous C from sediments into the water column after storm events in small stratified lakes (Bartosiewicz et al., 2015; Czikowsky et al., 2018; Vachon and Del Giorgio, 2014). However, small lakes account for 25% to 35% of the total area of the earth's surface lakes (Cole et al., 2007; Downing et al., 2006; Raymond et al., 2013). Compared to the case in larger lakes, C fluxes in small lakes remain uncertain because small lakes have usually been ignored in calculations of C flux on a global scale (Cole et al., 2007; Raymond et al., 2013). Thus, elucidation of the C fluxes in small lakes in extreme climates is key to optimizing estimations of global C fluxes in extreme climates.

Understanding the influences of physical, hydrological, and biogeochemical processes on the fate of C fluxes in smaller lake ecosystems is challenging work (Aufdenkampe et al., 2011; Cole et al., 2007; Raymond et al., 2013; Tranvik et al., 2009; Vachon et al., 2021; Woolway et al., 2018). This is not only because of difficulties in measurement but also because of the dynamics and interactions between factors and processes associated with C fluxes. Dissolved inorganic carbon (DIC) concentration is an important factor in estimating CO_2 fluxes within lake ecosystems (Smith, 1985). Among C fluxes in a freshwater body, the partial pressure of CO_2 (pCO_2), defined as CO_2 emission across the air–water interface, is affected by dissolved inorganic C (DIC), water temperature, wind speed, and pH (Jähne et al., 1987; Smith, 1985).

River inflows, sediment, and respiration contribute to DIC loading into lakes (Hope et al., 2004; Vachon et al., 2021); simultaneously, autotrophic organisms, such as planktons and submerged vegetation, capture DIC via photosynthesis (Amaral et al., 2022; Nakayama et al., 2020; Nakayama et al., 2022). Moreover, calcification and mineralization may consume dissolved oxygen within water, inducing uncertainty in pCO_2 estimation (Hanson et al., 2015; Lin et al., 2022; Nakayama et al., 2022). Dissolved organic carbon (DOC) might contribute to CO_2 emission from lake water to the atmosphere through mineralization and remineralization within lake ecosystems (Hanson et al., 2015; Sobek et al., 2005). In subtropical freshwater ecosystems, DOC concentration is a vital factor in describing variances in mineralization and remineralization rates for dissolved C (Lin et al., 2022; Shih et al., 2019). Kossin et al. (2013) investigated global storm events with an accumulated rainfall of about 50 mm, which is approximately 10 %–40% of precipitation in a subtropical typhoon event. Other studies have found that typhoon disturbances quickly mix, renew, or dilute the water in small subtropical lakes (Kimura et al., 2012; Kimura et al., 2017; Lin et al., 2022). Therefore, investigating the magnitudes of DIC and DOC during typhoon disturbances is understanding the seasonal regimes and to estimating C fluxes in small subtropical lakes.

Typhoons' effects on C fluxes were previously studied in a small, two-layer stratified, subtropical lake, Yuan–Yang Lake (YYL) (Chiu et al., 2020; Jones et al., 2009; Lin et al., 2021; Lin et al., 2022). Jones et al. (2009) used the conceptual hydrology model and sensor data to estimate CO_2 emission in YYL during typhoon disturbances that occurred in October 2004: 2.2 to 2.7 g C m^{-2} d^{-1} of CO_2 was released into the atmosphere. CO_2 emissions into the atmosphere were recorded at around 3.0 to 3.7 g C m^{-2} d^{-1} because of substantial loads of terrestrial C via river inflows after strong typhoons in YYL (Chiu et al., 2020).In particular , vertical mixing, thermal stratification, and river retention regimes were found to be essential physical processes in the C fluxes in YYL (Lin et al., 2021; Lin et al., 2022). These studies suggest that river intrusion and thermal stratification are key factors shaping the seasonal and interannual patterns of C fluxes during typhoon disturbances. River intrusion not only controls the C fluxes, algal biomass, and nutrient loading, but also influences the length of stratification and hydraulic retention times (Lin et al., 2021; Lin et al., 2022; Maranger et al., 2018; Nakayama et al., 2020; Olsson et al., 2022a; Olsson et al., 2022b; Zwart et al., 2017; Vachon and Del Giorgio, 2014). We hypothesized that allochthonous C loading and river inflow intrusion may affect DIC and DOC distributions (Fig. 1).Further, autochthonous processes in small subtropical lakes, such as algal photosynthesis, remineralization, and vertical transportation, must also be considered (Fig. 1). Here, we tested our hypothesis developing two-layer conceptual C models to assess C flux responses to typhoon disturbances in small subtropical lakes.

2. Materials and methods

2.1 Study site

YYL is a shallow (mean water depth: 4.3 m) and oligotrophic (total phosphorous: 10-20 μg-P L^{-1}; total nitrogen: 20-60 μg-N L^{-1}) subtropical mountain lake (Chou et al., 2000; Tsai et al., 2008; Wu et al., 2001) on Chi-Lan Mountain at around 1,640 asl in north-central Taiwan (24.58° N, 121.40° E) (**Figure 2)**. Its water is brown because of its humic acid content (colored dissolved organic matter: 20–50 ppb QSE; with specific ultraviolet absorbance at 254 nm assessed by a portable fluorometer (model C3; Turner Designs, Sunnyvale, CA, USA); mean pH: 5.4). YYL is surrounded by old-growth trees such as *Chamaecyparis formosensis*, *Chamaecyparis obtusa* var. *formosana*, and *Rhododendron formosanum* Heiml (Chou et al., 2000). Annual precipitation is over 3,000 mm yr^{-1}, and typhoon precipitation contributes up to half of the total precipitation in YYL (Chang et al., 2007; Lai et al., 2006). Due to the rapid renewal of the water body, the water retention time (or residence time) was around 4.4 days in typhoon Megi from 27 September to 1 October 2016 (Lin et al., 2022). The water surface temperature ranges from 15 to 25 ˚C during March to August, and the water column overturns in September (Kimura et al., 2012; Kimura et al., 2017; Lin et al., 2021). The concentrations of dissolved C (Lin et al., 2021), nutrients (Chiu et al., 2020; Tsai et al., 2008) and organisms (Shade et al., 2011) increase within YYL from autumn to winter. YYL has been registered as a long-term ecological study site by the Ministry of Science and Technology (MOST) of Taiwan since 1992 and became part of the Global Lake Ecological Observatory Network (GLEON) in 2004.

2.2 Water sampling and chemical analysis

We collected water quality samples (DOC, DIC, and Chl. *a*) at water depths of 0.04, 0.50, 1.00, 2.00, and 3.50 m at the buoy site (Fig. 2). We also measured the water surfaces of six river inflows and an outflow monthly using a horizontal van Dorn bottle (2.20 L, acrylic) from January 2015 to December 2018 (Fig. 2). These samples were collected using a portable hand pump and glass microfiber filter papers (47 mm GF/F, nominal pore size 0.70 μm; Whatman, Maidstone, Kent, UK) to obtain filtrate samples. Water samples were stored at around 4°C in a refrigerator until analysis. Samples were analyzed using an infrared gas detector to detect DIC and DOC concentrations with persulfate digestion (model 1088 Rotary TOC autosampler; OI Analytical, College Station, TX, USA). The filter papers were kept in opaque bottles at around -25 °C in a refrigerator until the samples were analyzed using a portable fluorometer (model 10-AU-005-CE; Turner Designs, Sunnyvale, CA, USA). The specific wavelengths were 430 nm (blue) and 662 nm (red). In the laboratory, the filter papers were extracted with methanol to obtain Chl. a concentration. These samples were analyzed for less than 72 h to prevent light and chemical degradation.

2.3 Data analysis and numerical modeling

Three water quality variables (DIC, DOC, and Chl a) were compared between different layers (upper and lower layers), years (typhoon years and non-typhoon years), and seasons (spring, summer, autumn, and winter). First, we separated our investigation data into typhoon years and non-typhoon years as described in Sect. 2.3.1. Next, we developed a conceptual equations model to generate continuous DIC and DOC data at the upper and lower layers as shown in **Figure 1**. This helped us understand the transportation, photosynthesis, and remineralization rates between seasons and between typhoon and non-typhoon years (see Sect. 2.3.2).

2.3.1 Typhoon and non-typhoon years

We collected meteorological data from a meteorological tower located about 1.0 km from YYL (Lin et al., 2021; Lin et al., 2022). Rainfall (model N-68; Nippon Electric Instrument, Tokyo, Japan) and wind speed (model 03001, R.M. Young, Traverse City, MI, USA) data were stored in a datalogger (model CR1000; Campbell Scientific, Logan, UT, USA) for every 10 min. River discharge (Q_{in}, m^3 d^{-1}) was estimated every 10 min using the rainfall data and a water depth meter (model HOBO U20; Onset Computer, Bourne, MA, USA) at the end of a river inflow (**Figure 2**) using the Manning formula. Transparency was estimated using Secchi disc data measured at local times (GMT+08:00) from 10:00 to 14:00.

As **Table 1** shows, four strong typhoons were recorded, contributing a total of 2,254 mm of precipitation in all 24 months of 2015 and 2016, accounting for 35.6% of the annual precipitation. However, no typhoon rainfall was recorded at YYL in 2017 and 2018; the total precipitation in that 2-year period was around 2,537 mm. There was no significant difference in average water depth between 2017 and 2018 (**Table 1**). The average discharge was less than 774 m^3 d^{-1} in 2017 and 2018. Thus, we considered 2015 and 2016 as typhoon years, and 2017 and 2018 as non-typhoon years.

2.3.2 Conceptual two-layer DIC and DOC model

Nakayama et al. (2010) successfully developed a conceptual two-layer dissolved oxygen model based on strong wind turbulence at Tokyo Bay. Lin et al. (2021) pointed out that thermal stratification that inhibits vertical C flux between the upper and lower layers in shallow stratified lakes makes it possible to develop conceptual two-layer C models (Lin et al., 2022; Nakayama et al., 2022), and the phytoplankton and remineralization effects on DIC and DOC fluxes ($d\mathrm{DIC}/dt$ and $d\mathrm{DOC}/dt$, mg-C L^{-1} d^{-1}) were considered in a conceptual two-layer equation model as shown in Equation 1– Equation 4. The fluxes in the upper layer (from the water surface to 2.5 m water depth) were calculated as follows:

$$V_U \frac{d\mathrm{DIC}_U}{dt} = Q_U \mathrm{DIC}_R - Q_{out} \mathrm{DIC}_U - V_U \alpha_{PU} Chl_U + V_U \alpha_{MU} DOC_U + A_I w_I (\mathrm{DIC}_L - \mathrm{DIC}_U) + Q_L \mathrm{DIC}_L - \frac{A_s F_{CO2}}{C_U} + Pa_U \tag{1}$$

$$V_U \frac{d\mathrm{DOC}_U}{dt} = Q_U \mathrm{DOC}_R - Q_{out} \mathrm{DOC}_U - V_U \alpha_{MU} DOC_U + A_I w_I (\mathrm{DOC}_L - \mathrm{DOC}_U) + Q_L \mathrm{DOC}_L + Pb_U \tag{2}$$

Those in the lower layer (from 2.5 to 4.0 m water depth) were calculated as follows:

$$V_L \frac{d\mathrm{DIC}_L}{dt} = Q_L \mathrm{DIC}_R - V_L \alpha_{PL} Chl_L + V_L \alpha_{ML} DOC_L + A_I w_I (\mathrm{DIC}_U - \mathrm{DIC}_L) - Q_L \mathrm{DIC}_L + \frac{A_B BF_{DIC}}{C_U} + Pa_L \tag{3}$$

$$V_L \frac{d\mathrm{DOC}_L}{dt} = Q_L \mathrm{DOC}_R - V_L \alpha_{ML} DOC_L + A_I w_I (\mathrm{DOC}_U - \mathrm{DOC}_L) - Q_L \mathrm{DOC}_L + Pb_L \tag{4}$$

$$V_{total} = V_U + V_L \tag{5}$$

$$Q_{in} = Q_U + Q_L \tag{6}$$

where, as shown in Table 2, total lake volume (V_{total}, 53,544 m^3) departs to the upper layer (V_U, 45,456 m^3) and to the lower layer (V_L, 8,808 m^3) (Equation 5), and where lake surface area (A_s) is 36,000 m^2 and the bottom of lake area (A_B) is 3,520 m^2. The interface is 2.5 m vertically, and the interface area (A_I) is 7,264 m^2 in YYL. The water depth is not only steady but also changes. However, the change in water depth ranged from 4.56 to 4.66 m during the typhoon period. Therefore, we can assume that the changes in lake volumes and areas were negligible. The C_U is a coefficient value (= 1,000) to establishing a standard unit for F_{CO2} (mg-C m^{-2} d^{-1}), considering the air–water CO_2 exchange by Fick's law as follows:

$$F_{CO2} = k_{CO2} \cdot K_H (pCO2_{water} - pCO2_{air}) \tag{7}$$

where k_{CO2} is the gas transfer velocity from empirical wind speed equations (Cole and Caraco, 1998; Jähne et al., 1987; Smith, 1985; Wanninkhof, 1992). K_H is Henry's coefficient calculated by water temperature empirical equations (Plummer and Busenberg, 1982). $pCO2_{air}$ (μatm) is the CO_2 partial pressure in the atmosphere using air pressure data (Lin et al., 2021; Lin et al., 2022), and the atmospheric CO_2 concentration is assumed to be 400 ppm. $pCO2_{water}$(μatm) is the CO_2 partial pressure at the water surface around 0.04 m water depth from water quality data (temperature, pH, DIC concentration at the water surface. The empirical equation (Cai and Wang, 1998) was also followed by Lin et al. (2021). F_{CO2} contributed approximately half of the net ecosystem production (NEP) across the water surface to the atmosphere in YYL (Lin et al., 2021). Further, because sediment carbon may be an important flux into shallow subtropical lakes, the sediment C flux (BF_{DIC}, BF_{DOC}, mg-C L^{-1}) in the lower layer was considered (Lin et al., 2022).

We assumed that the river discharge and outflow discharge (Q_{out}, m^3 d^{-1}) are in a quasi–steady state ($Q_{in} = Q_{out}$), dividing into upper discharge (Q_U, m^3 d^{-1}) and lower discharge (Q_L, m^3 d^{-1}) (Equation 6). Lin et al. (2021) showed that the buoyancy frequencies in YYL were 0.011 ± 0.004 s^{-1}, 0.013 ± 0.004 s^{-1}, 0.006 ± 0.003 s^{-1}, and 0.007 ± 0.004 s^{-1} from spring (March–May), summer (June–August), autumn (September–November), and winter (December–February), respectively, inhibiting the vertical profile of DIC mixed due to stratification. We estimated the percentages of Q_U and Q_L based on the buoyancy frequency following Lin et al. (2020 and 2022). Q_U values were 75%, 80%, 45%, and 50% of Q_{in} for spring to winter, and Q_L values were 25%, 20%, 55%, and 50% of Q_{in}. The physical and biogeochemical regimes under climate change remain uncertain, such as biological compositions, mixing regimes, morphometric characteristics, and air–water energy fluxes (evaporation and transpiration) (Woolway et al., 2020). To simulate extreme climate scenarios, we shifted the ratio of Q_{in} for each season and tested the river intrusion hypothesis (Fig. 1). We established two extreme conditions: *Level 1* and *Level 2*. *Level 2* is the more extreme condition: Q_U is 80% (spring), 85% (summer), 50% (autumn), and 50% (winter) of Q_{in}; Q_L is 20% (spring), 15% (summer), 50% (autumn), and 50% (winter) of Q_{in}. *Level 1* is the condition between the present and the *Level 2* condition: Q_U is 77% (spring), 82% (summer), 47% (autumn), and 50% (winter) of Q_{in}; Q_L is 23% (spring), 18% (summer), 53% (autumn), 50% (winter) of Q_{in}.

The contributions of photosynthesis production depended on the chlorophyll *a* concentration (Chl_U, Chl_L, mg L^{-1}) and on the absorption coefficients in the upper layer (α_{PU}, d^{-1}) and lower layer (α_{PL}, d^{-1}). The coefficients of DOC remineralization rates in the upper layer (α_{MU}, d^{-1}) and lower layer (α_{ML}, d^{-1}) were also considered in the conceptual models. The Pa_U, Pa_L, Pb_U, and Pb_L are constants in the conceptual models. To obtain unknown values (α_{PU}, α_{MU}, α_{PL}, α_{MU}, α_{ML}, w_I, BF_{DIC}, BF_{DOC}, Pa_U, Pa_L, Pb_U, and Pb_L), we applied multiple linear regression analysis. Further, these unknown values were tested by trial and error to obtain the parameters of the *best-fit* condition (Nakayama et al., 2022), dividing the seasonal and nonseasonal serranoids to learn the seasonal differences. The same parameters of the *best-fit* condition were used to obtain the extreme conditions for *Level 1* and *Level 2*. We used the coefficient of determination (R^2) and the Nash–Sutcliffe model efficiency coefficient (NSE)

(Nash and Sutcliffe, 1970) to quantify the performance of the equation model with DIC and DOC sampling data (observation data) for each simulation.

2.3.3 DIC and DOC fluxes

VNt ecosystem production was defined as the difference between primary production and ecological respiration (NEP = GPP - ER) due to photosynthesis and respiration via biota (Dodds and Whiles, 2020). Given that we assumed that the C fluxes were dependent on the river inflows in YYL (Fig. 2), we estimated the NEP by end-member analysis using the C concentration of the river inflow and outflow (Lin et al., 2021; Nakayama et al., 2020) by following Equation 8–Equation 11. The upper layer NEP of DIC flux (mg C d^{-1}) was obtained from Equation 1 as follows:

$$\begin{aligned}
\text{Upper flux}_{\text{DIC}} &= C_U \alpha_{PU} Chl_U - C_U \alpha_{MU} DOC_U - C_U \frac{A_I w_I (\text{DIC}_L - \text{DIC}_U)}{V_U} - C_U \frac{Pa_U}{V_U} \\
&= C_U \frac{Q_U \text{DIC}_R + Q_L \text{DIC}_L - Q_{out} \text{DIC}_U}{V_U} - \frac{A_S}{V_U} F_{CO2} \\
&= C_U \frac{1}{t_{rU}} \left(\frac{Q_U}{Q_{in}} \text{DIC}_R + \frac{Q_L}{Q_{in}} \text{DIC}_L - \text{DIC}_U \right) - F_C \\
t_{rU} &= \frac{V_U}{Q_{in}}
\end{aligned} \tag{8}$$

The upper layer flux of DOC flux (mg C m^{-3} d^{-1}) was estimated from Equation 2:

$$\begin{aligned}
\text{Upper flux}_{\text{DOC}} &= C_U \alpha_{MU} DOC_U - C_U \frac{A_I w_I (\text{DOC}_L - \text{DOC}_U)}{V_U} - C_U \frac{Pb_U}{V_U} \\
&= C_U \frac{Q_U \text{DOC}_R + Q_L \text{DOC}_L - Q_{out} \text{DOC}_U}{V_U} \\
&= C_U \frac{1}{t_{rU}} \left(\frac{Q_U}{Q_{in}} \text{DOC}_R + \frac{Q_L}{Q_{in}} \text{DOC}_L - \text{DOC}_U \right)
\end{aligned} \tag{9}$$

The lowerlayer flux of DIC flux (mg C m^{-3} d^{-1}) was estimated from Equation 3:

$$\text{Lower flux}_{\text{DIC}} = C_U \alpha_{PL} Chl_L - C_U \alpha_{ML} DOC_L - C_U \frac{A_I w_I (\text{DIC}_U - \text{DIC}_L)}{V_L} - \frac{A_B BF_{DIC}}{V_L}$$
$$- C_U \frac{Pa_L}{V_L} = C_U \frac{Q_L(\text{DIC}_R - \text{DIC}_L)}{V_L} = C_U \frac{1}{t_{rL}} \frac{Q_L}{Q_{in}} (\text{DIC}_R - \text{DIC}_L) \tag{10}$$
$$t_{rL} = \frac{V_L}{Q_{in}}$$

The lowerlayer fluxof DOC flux (mg C m^{-3} d^{-1}) was estimated from Equation 4:

$$\text{Lower NEP}_{\text{DOC}} = C_U \alpha_{ML} DOC_L - C_U \frac{A_I w_I (\text{DOC}_U - \text{DOC}_L)}{V_L} - \frac{A_B BF_{DOC}}{V_L} - C_U \frac{Pb_L}{V_L}$$
$$= C_U \frac{Q_L(\text{DOC}_R - \text{DOC}_L)}{V_L} = C_U \frac{1}{t_{rL}} \frac{Q_L}{Q_{in}} (\text{DOC}_R - \text{DOC}_L) \tag{11}$$

Thus, the total flux of DIC and DOC are:

$$\text{Flux}_{\text{DIC}} = \frac{V_U \text{Upper flux}_{\text{DIC}} + V_L \text{Lower flux}_{\text{DIC}}}{V_{total}} \tag{12}$$

$$\text{Flux}_{\text{DOC}} = \frac{V_U \text{Upper flux}_{\text{DOC}} + V_L \text{Lower flux}_{\text{DOC}}}{V_{total}} \tag{13}$$

where, F_C is $\frac{A_S}{V_U} F_{CO2}$ and t_{rU}, t_{rL} are residence times (*d*) in the upper and lower layers, respectively. These parameters were used for the *best-fit* condition as shown in Table 2.

3. Results

3.1 DIC, DOC, and Chl. a concentrations in the typhoon and non-typhoon years

The results of the comparisons between the two periods of typhoon years demonstrated that there were no significant differences in DIC, DOC, and Chl *a* concentration between the layers in the typhoon years 2015 and 2016; however, all these parameters differed significantly between the layers in the typhoon years 2017 and 2018 (Fig. 3). The average DIC_U was 1.23 mg-C L^{-1}, and DIC_L was 3.66 mg-C L^{-1}; the average DOC_U was 5.87 mg-C L^{-1}, and DOC_L was 8.02 mg-C L^{-1}; and the Chl_U and Chl_L were 18.5 µg-C L^{-1} 2.13 µg-C L^{-1}, respectively (Fig. 3). However, the t-test results showed no significant differences in DIC, DOC, and Chl. *a* concentrations (p-values ≥ 0.05 that show no significant differences in DIC data among seasons in the typhoon years) (Fig. 4 a). However, the DOC concentration showed significant differences between seasons in the typhoon years (Fig. 4 c-d). No significant differences between Chl_U and Chl_L were observed among the seasons (Fig. 4e-f) , whereas the standard deviations (SD) of DIC and DOC were higher in summer and autumn (Fig. 4) due to terrestrial C loading (Chiu et al., 2020). In summer, the SD values of DIC_U and DOC_U were 3.51 mg-C L^{-1} and 3.69 mg-C L^{-1}, respectively (Fig. 4a, c, e). In autumn, DIC_L and DOC_L had the highest SD (4.06 and 4.17 mg-C L^{-1}, respectively) (Fig. 4b, d). Notably, the maximums of DIC_U and DOC_U were 7.06 and 15.6 mg-C L^{-1} and those of DIC_L and DOC_L were 10.9 and 19.8 mg-C L^{-1}, respectively, in the typhoon years (Fig. 4 a-d).

Positive Pearson correlations of 0.45 to 0.80 were observed between the DOC and DIC in the typhoon years (Fig. 5a). In the non-typhoon years, the upper layer DIC_L was the only variable negatively correlated with DOC in the upper and lower layers (Fig. 5b). The DIC of the lower layer was positively correlated with the Chl_L due to the abundant respiration in the lower layer (Fig. 5).

3.2 Performance of conceptual two-layer DIC and DOC models

The results for the typhoon years demonstrated that most of the seasonal scenarios were better fitting than the nonseasonal scenarios (Fig. 6). Under the seasonal scenarios, the DIC_U was around 1.5 to 5.0 mg-C L^{-1} (Fig. 6a-b) and DIC_L was around 5.0 mg-C L^{-1} stably (Fig. 6d**)**. However, the NSE of DIC_L was 0.73 under the nonseasonal scenarios, which was higher than seasonal scenarios (NSE = 0.71) (Table 2), because DIC_L was elevated dramatically, by 40 mg-C L^{-1}, under the nonseasonal scenarios during the 2016 typhoon period (**Fig. 6c**). In the non-typhoon years (2017–2018), the *best-fit* values of DIC_U and DIC_L did not differ significantly between the seasonal and nonseasonal scenarios (R^2 and NSE were around 0.40 and 0.70, respectively). These results demonstrated that DIC_U and DIC_L in the typhoon years must use the seasonal scenarios, whereas in the non-typhoon years they should use the nonseasonal scenarios. On the other hand, the DOC under the seasonal scenarios fit our observation data (R^2 = 0.91, 0.46 and NSE = 0.95, 0.73 for DOC_U, DOC_L, respectively) (Fig. 6e-h, Table 3). Thus, the results suggested that the DOC_U and DOC_L must use the seasonal scenarios in both the typhoon and non-typhoon years.

As shown in **T**able 3, the parameters for the conceptual two-layer DIC and DOC models showed different regimes between the typhoon and non-typhoon years. In the typhoon years, the photosynthesis absorption rates coefficients (α_{PU}, α_{PL}) were negative (photosynthesis < respiration) for each season. YYL was a C source due to a large allochthonous C loading during typhoons; the respiration was elevated by around 30- to 150-fold from summer to autumn. However, the transportation coefficients (w_I) were higher in autumn than in the other seasons (Table 3) due to weak stratification and large C loading during typhoons. Further, the higher remineralization rates during typhoon disturbances from summer to autumn resulted in positive α_{MU} and α_{ML}. In the non-typhoon years, the remineralization rates were negative (Table 3). Thus, the results suggest that the conceptual two-layer C models may reasonably fit the observation data.

3.3 Interannual and seasonal NEP in YYL

The typhoon disturbances in summer and autumn played an important role in promoting the C released by YYL (Table 4). Overall, YYL released 245 mg C m^{-3} d^{-1} of DIC and 415 mg C m^{-3} d^{-1} of DOC during the typhoon years; during the non-typhoon years, it released 51.7 mg C m^{-3} d^{-1} of DIC and 22.8 mg C m^{-3} d^{-1} of DOC (Table 4). The average F_C was one to two times larger than $\mathrm{Flux_{DIC}}$, and 219 and 133 mg C m^{-3} d^{-1} were released from YYL into the atmosphere in the typhoon and non-typhoon years, respectively (Table 4). In summer, the upper layer DIC and DOC consumed approximately 3.7 times more DIC in the typhoon years than in the non-typhoon years (Table 4). In autumn, 216 mgC d^{-1} of upper layer DIC was released; however, 46.1 mg C m^{-3} $d^{-1}$of upper layer DOC was produced in the typhoon years. The upper layer $\mathrm{Flux_{DIC}}$ was negative in the autumn of the typhoon years, when 268 mg C m^{-3} d^{-1} more F_C was released compared to the non-typhoon years. In addition, the lower layer was most released of C into the outflow; however, the fluxes in the lower layer was more than twice as high in the summer as in the autumn of the typhoon years (Table 4). The average of total $\mathrm{Flux_{DIC}}$ was 3.14 times more released C in the typhoon than in the non-typhoon years; The average of total $\mathrm{NEP_{DOC}}$ was increased 62.3 mg C m^{-3} d^{-1} of DOC between the typhoon years and non-typhoon years due to the over ten-times higher flux in the upper layer (Table 4).

The ratios of DIC and DOC concentrations reveal the magnitudes of allochthonous DOC loading into YYL (Shih et al., 2019; Walvoord and Striegl, 2007), and the upper and lower layers show different patterns. In the typhoon years, the upper layer ratios decreased (higher DOC loading) from summer to autumn, whereas in the lower layer, the DIC:DOC decreased from autumn to winter. In the non-typhoon years, the autumn DIC:DOC ratio was the lowest, around 0.216 to 0.351 (Table 4).

3.4 Interannual responses of DIC and DOC to typhoons

We simulated the responses of DIC and DOC flux to typhoons using conceptual two-layer C models. The results showed that the DIC was more sensitive to typhoon disturbances than DOC under the scenarios of *Level 1* and *Level 2* (Fig. 7-9). Overall, the C level declined in the upper layers but increased in the lower layers (Fig. 7). DIC and DOC in the upper layer tended to decline from 1.0 (*Level 1*) to 2.0 mg-C L^{-1} (*Level 2*) (Fig. 7a, c); however, they increased to 10.0 and 20.0 mg-C L^{-1} in the lower layer under *Level 1* and *Level 2*, respectively (Fig. 7b, d).

The DIC concentration in the upper layer was significantly lower in typhoon than in the non-typhoon years during spring and autumn under *Level 2* (Fig. 8a-c). Under the *best-fit* and *Level 1* conditions, the DIC concentrations decreased significantly from winter to spring (Fig. 8c-d). The lower layer DIC values under the *best-fit* and *Level 1* conditions differed significantly between the typhoon and non-typhoon years (Fig. 8e-h). The DIC of the lower layer under *Level 2* differed significantly from winter to spring only (Fig. 8e, h). However, the upper layer DOC showed significant typhoon responses for each condition from winter to spring (Fig. 9a, d). The DOC of the upper layer tended to differ more significantly under the extreme climates from summer to autumn (Fig. 9b-c). The DOC of the lower layer showed different typhoon responses between the spring and the other seasons (Fig. 9 e-h).

4. Discussion

Annual total precipitation was 40% higher in typhoon years than in non-typhoon years (Table 1).Water retention and typhoon-induced upwelling control the dynamics of DIC and DOC during the summer and autumn (Chiu et al., 2020; Jones et al., 2009; Tsai et al., 2008; Tsai et al., 2011). Typhoon-induced upwelling affected water quality data differently between the upper and lower layers (Fig. 3). DIC, DOC, and Chl. a concentrations differ significantly between upper and lower layers in the typhoon years (Fig. 3) due to thermal stratification (Chiu et al., 2020; Lin et al., 2022; Tsai et al., 2008; Tsai et al., 2011). Further, the abundance of organisms leads to intensive respirations in the lower layers during the non-typhoon period; for example, an anoxic condition at the hypolimnion may affect C mineralization and remineralization rates in non-typhoon years (Carey et al., 2022; Chiu et al., 2020; Lin et al., 2022; Shade et al., 2010; Shade et al., 2011). Therefore, these physical and biogeochemical processes might describe different patterns between the upper and lower layers, as revealed by the Pearson correlations (Fig. 5).

Thermal stratification and allochthonous C loading may drive the responses of fluxes to typhoons in YYL. In the typhoon years, the absolute values of fluxes were higher than in the non-typhoon years (Table 4). We found that precipitation from typhoons loaded large amounts of allochthonous C into YYL during summer and autumn, which might describe the higher fluxes in autumn compared to other seasons (Table 4). Typhoons dramatically changed the seasonal and interannual patterns of DIC fluxes due to river intrusion (Fig. 7a–b; Fig. 8), which corresponds to our hypothesis (Fig. 1) and to the results of previous studies (Chiu et al., 2020; Lin et al., 2021; Lin et al., 2022). In summer, the spatial differences in DIC and DOC between layers were inhibited due to strong thermal stratification, describing the positive upper net primary production and lower negative net primary production (Lin et al., 2021).The thermal stratification and anoxic condition may have been controlled by the seasonal and interannual patterns of DIC and DOC fluxes in the non-typhoon years (Tables 3–4; Fig. 6). Additionally, because of the absence of typhoon-induced mixing and allochthonous C loading, the absolute values of total fluxes in the non-typhoon years were less than those the non-typhoon years (Table 4). These results suggested that the allochthonous C loading was the most crucial factor for DIC and DOC fluxes in the typhoon years; on the other hand, the transportation rate shaped the seasonal C due to thermal stratification in the non-typhoon years.

Water temperature might be a crucial driver in controlling C fluxes in YYL (Chiu et al., 2020; Lin et al., 2021; Lin et al., 2022). We found that the fluxes and F_{CO2} in summer were usually higher than in winter (Tables 3–4) due to the higher levels of photosynthesis, remineralization, and strength of thermal stratification (Lin et al., 2021; Lin et al., 2022). With the conceptual two-layer C models (Table 3), photosynthesis absorption (α_{PU}, α_{PL}), remineralization (α_{MU}, α_{ML}), and transportation (w_I) well represented the seasonal variations of DIC and DOC data. These parameters of the conceptual two-layer C models appeared in reasonable patterns (Table 3). The higher remineralization and photosynthesis rates resulted in higher absolute values of fluxes in the autumn of the typhoon years (Tables 3-4). In the non-typhoon years, the photosynthesis rates contributed to the total fluxes (Tables 3-4). Moreover, without the typhoon-induced mixing and refreshing of the water column, anoxic conditions may occur (Carey et al., 2022; Vachon et al., 2021), which could result in negative remineralization rates in non-typhoon years. Thus, the conceptual two-layer C models well characterizes the seasonal and interannual responses of DIC and DOC fluxes to typhoons in YYL.

Under extreme weather conditions, *Level 2* usually shifted to different typhoon responses for each season (Fig. 8-9) due to extreme river intrusions. DIC changes more significantly than DOC under *Level 1* and *Level 2* (Fig. 7-9), because the photosynthesis, transportation, and remineralization rates may crucially affect the seasonal and interannual patterns of DOC as well (Fig. 1). Moreover, we compared the fluxes with different model conditions as shown in Fig. 10, demonstrating that the responses of $Flux_{DIC}$ to typhoons differed dramatically between *Level 1* and *Level 2* (Fig. 10a-c); especially, the Upper $Flux_{DIC}$ released more C in the typhoon years and absorbed more C in the non-typhoon years than *Obs* (Fig. 10a). Not only were the absolute values of $Flux_{DIC}$ over 3 times higher in the typhoon than the non-typhoon years (Table 4), but SD was higher in the typhoon years as well (Fig. 10). Additionally, the F_C was 43 % higher (~83 mg C m^{-3} d^{-1}) in typhoon years than in non-typhoon years (**Table 4**). Therefore, the typhoon disturbances control DIC loading and C emissions in YYL, which is consistent with our previous studies (Chiu et al., 2020; Lin et al., 2021; Lin et al., 2022).

However, DOC fluxes changed less under *Level 1* and *Level 2* (Fig. 10d-f), a finding that is consistent with our continuous DOC data (Fig. 7c-d). Processes such as respiration, mineralization, and sediment burial may impact DOC fluxes (Bartosiewicz et al., 2015; Hanson et al., 2015; Maranger et al., 2018). To our knowledge, bio-photochemical mineralization and degradation may play a key role in shaping C fluxes because colored DOC reduces ultraviolet radiation (UVR) and active photosynthetic radiation (PAR) (Allesson et al., 2021; Chiu et al., 2020; Schindler et al., 1996; Scully et al., 1996; Williamson et al., 1999). Ejarque et al. (2021) also successfully developed a conceptual one-layer model of DOC and DIC, considering bacterial respiration, photo-mineralization and degradation in a temperate mountain lake. In addition,, Nagatomo et al. (2023) suggested that the DIC might be underestimated if submerged vegetation is ignored. Thus, we suggest that photo-biochemical processes (such as photo-mineralization) and submerged vegetation should be considered in the upper layer to clarify and validate the responses of the total C fluxes under extreme climates in a two-layer stratified lake.

5. Conclusions

Our conceptual two-layer C model revealed that allochthonous and autochthonous processes both accounted for C flux responses to typhoon disturbances on seasonal and interannual scales by applying our proposed two-layer conceptual C model. Without typhoons, the strength of thermal stratification was the primary determinants the seasonal and interannual patterns of DIC and DOC concentrations data and typhoon-induced fluxes upwelling and loading facilitated 102.2 mg-DIC m^{-3} d^{-1} and 62.3 mg-DOC m^{-3} d^{-1} in YYL, respectively (Table 4). We successfully developed two-layer conceptual C models to obtain continuous DIC and DOC data in YYL and to simulate extreme conditions. The changes in seasonal river intrusion regimes in YYL resulted in a 3-fold higher total $Flux_{DIC}$ in the typhoon years than in the non-typhoon years. However, our model should be improved under extreme climate scenarios by considering other autochthonous processes, such as sediment burial, photo-biochemical processes, and anoxic conditions. The present results suggest that physical processes (river intrusion and vertical transportation) and biogeochemical processes (mineralization, photosynthesis, and respiration) in a subtropical small lake account for the C flux responses to typhoons on seasonal and interannual time scales.

Competing interests

The authors have no conflicts of interest to report.

Acknowledgements

The authors thank YS Hsueh, LC Jiang, and TY Chen for their help with the water sample collection and chemistry analysis. This work was supported by the Japan Society for the Promotion of Science (JSPS) under grant nos. 22H05726, 22H01601, and 18KK0119 for K Nakayama; and by the Academia Sinica, Taiwan (AS-103-TP-B15), Ministry of Science and Technology, Taiwan (MOST 106-2621-M-239-001, MOST 107-2621-M-239-001, MOST 108-2621-M-239-001) for CY Chiu and JW Tsai. This study benefited from participation in the Global Lakes Ecological Observatory Network (GLEON).

Hao-Chi Lin: Conceptualization, Methodology, Investigation, Formal analysis, Writing – original draft. Keisuke Nakayama: Methodology, Supervision, Writing – review & editing, Conceptualization. Jeng-Wei Tsai: Investigation, Funding acquisition, Writing –review & editing. Chih-Yu Chiu: Funding acquisition, Writing – review & editing.

Data availability

The data that support the findings of this study are adopted from our previous works, including Chiu et al. (2020), Lin et al. (2021), and Lin et al. (2022).

References

Allesson, L., Koehler, B., Thrane, J.-E., Andersen, T., and Hessen, D. O.: The role of photomineralization for CO_2 emissions in boreal lakes along a gradient of dissolved organic matter, Limnol. Oceanogr., 66, 158–170, https://doi.org/10.1002/lno.11594, 2021.

Amaral, J. H. F., Melack, J. M., Barbosa, P. M., Borges, A. V., Kasper, D., Cortés, A. C., Zhou, W., MacIntyre, S., and Forsberg, B. R.: Inundation, Hydrodynamics and Vegetation Influence Carbon Dioxide Concentrations in Amazon Floodplain Lakes, Ecosystems, 25, 911–930, https://doi.org/10.1007/s10021-021-00692-y, 2022.

Aufdenkampe, A. K., Mayorga, E., Raymond, P. A., Melack, J. M., Doney, S. C., Alin, S. R., Aalto, R. E., and Yoo, K.: Riverine coupling of biogeochemical cycles between land, oceans, and atmosphere, Front. Ecol. Environ., 9, 53–60, https://doi.org/10.1890/100014, 2011.

Bartosiewicz, M., Laurion, I., and MacIntyre, S.: Greenhouse gas emission and storage in a small shallow lake, Hydrobiologia, 757, 101–115, https://doi.org/10.1007/s10750-015-2240-2, 2015.

Cai, W.-J. and Wang, Y.: The chemistry, fluxes, and sources of carbon dioxide in the estuarine waters of the Satilla and Altamaha Rivers, Georgia, Limnol. Oceanogr., 43, 657–668, https://doi.org/10.4319/lo.1998.43.4.0657, 1998.

Carey, C. C., Hanson, P. C., Thomas, R. Q., Gerling, A. B., Hounshell, A. G., Lewis, A. S. L., Lofton, M. E., McClure, R. P., Wander, H. L., Woelmer, W. M., Niederlehner, B. R., and Schreiber, M. E.: Anoxia decreases the magnitude of the carbon, nitrogen, and phosphorus sink in freshwaters, Glob. Change Biol., https://doi.org/10.1111/gcb.16228, 2022.

Chang, S.-C., Wang, C.-P., Feng, C.-M., Rees, R., Hell, U., and Matzner, E.: Soil fluxes of mineral elements and dissolved organic matter following manipulation of leaf litter input in a Taiwan Chamaecyparis forest, For. Ecol. Manag., 242, 133–141, https://doi.org/10.1016/j.foreco.2007.01.025, 2007.

Chiu, C.-Y., Jones, J. R., Rusak, J. A., Lin, H.-C., Nakayama, K., Kratz, T. K., Liu, W.-C., Tang, S.-L., and Tsai, J.-W.: Terrestrial loads of dissolved organic matter drive inter-annual carbon flux in subtropical lakes during times of drought, Sci. Total Environ, 717, 137052, https://doi.org/10.1016/j.scitotenv.2020.137052, 2020.

Chou, C.-H., Chen, T.-Y., Liao, C.-C., and Peng, C.-I.: Long-term ecological research in the Yuanyang Lake forest ecosystem I. Vegetation composition and analysis, Bot. Bull. Acad. Sin., 41, 61–72, 2000.

Cole, J. J. and Caraco, N. F.: Atmospheric exchange of carbon dioxide in a low-wind oligotrophic lake measured by the addition of SF_6, Limnol. Oceanogr., 43, 647–656, https://doi.org/10.4319/lo.1998.43.4.0647, 1998.

Cole, J. J., Prairie, Y. T., Caraco, N. F., McDowell, W. H., Tranvik, L. J., Striegl, R. G., Duarte, C. M., Kortelainen, P., Downing, J. A., Middelburg, J. J., and Melack, J.: Plumbing the Global Carbon Cycle: Integrating Inland Waters into the Terrestrial Carbon Budget, Ecosystems, 10, 172–185, https://doi.org/10.1007/s10021-006-9013-8, 2007.

Czikowsky, M. J., MacIntyre, S., Tedford, E. W., Vidal, J., and Miller, S. D.: Effects of Wind and Buoyancy on Carbon Dioxide Distribution and Air-Water Flux of a Stratified Temperate Lake, J. Geophys. Res. Biogeosci., 123, 2305–2322, https://doi.org/10.1029/2017JG004209, 2018.

Dodds, W. K. and Whiles, M. R.: Freshwater Ecology: Concepts and Environmental Applications of Limnology, Third Edition, Elsevier, United Kingdom, 748-762, 2020.

Doubek, J. P., Anneville, O., Dur, G., Lewandowska, A. M., Patil, V. P., Rusak, J. A., Salmaso, N., Seltmann, C. T., Straile, D., Urrutia-Cordero, P., Venail, P., Adrian, R., Alfonso, M. B., DeGasperi, C. L., Eyto, E., Feuchtmayr, H., Gaiser, E. E., Girdner, S. F., Graham, J. L., Grossart, H.-P., Hejzlar, J., Jacquet, S., Kirillin, G., Llames, M. E., Matsuzaki, S.-I. S., Nodine, E. R., Piccolo, M. C., Pierson, D. C., Rimmer, A., Rudstam, L. G., Sadro, S., Swain, H. M., Thackeray, S. J., Thiery, W., Verburg, P., Zohary, T., and Stockwell, J. D.: The extent and variability of storm-induced temperature changes in lakes measured with long-term and high-frequency data, Limnol. Oceanogr., 66, 1979–1992, https://doi.org/10.1002/lno.11739, 2021.

Douville, H., Raghavan, K., Renwick, J., Allan, R. P., Arias, P. A., Barlow, M., Cerezo-Mota, R., Cherchi, A., Gan, T. Y., Gergis, J., Jiang, D., Khan, A., Mba, W. P., Rosenfeld, D., Tierney, J., and Zolina, O.: Water cycle changes, Cambridge University Press, Climate Change 2021: The Physical Science Basis. Contribution of Working Group I to 45 the Sixth Assessment Report of the Intergovernmental Panel on Climate Change, 2021.

Downing, J. A., Prairie, Y. T., Cole, J. J., Duarte, C. M., Tranvik, L. J., Striegl, R. G., McDowell, W. H., Kortelainen, P., Caraco, N. F., Melack, J. M., and Middelburg, J. J.: The global abundance and size distribution of lakes, ponds, and impoundments, Limnol. Oceanogr., 51, 2388–2397, https://doi.org/10.4319/lo.2006.51.5.2388, 2006.

Ejarque, E., Scholz, K., Wohlfahrt, G., Battin, T. J., Kainz, M. J., and Schelker, J.: Hydrology controls the carbon mass balance of a mountain lake in the eastern European Alps, Limnol. Oceanogr., 66, 2110–2125, https://doi.org/10.1002/lno.11712, 2021.

Engel, F., Farrell, K. J., McCullough, I. M., Scordo, F., Denfeld, B. A., Dugan, H. A., Eyto, E. de, Hanson, P. C., McClure, R. P., Nõges, P., Nõges, T., Ryder, E., Weathers, K. C., and Weyhenmeyer, G. A.: A lake classification concept for a more accurate global estimate of the dissolved inorganic carbon export from terrestrial ecosystems to inland waters, Sci. Nat., 105, 25, https://doi.org/10.1007/s00114-018-1547-z, 2018.

Hanson, P. C., Pace, M. L., Carpenter, S. R., Cole, J. J., and Stanley, E. H.: Integrating Landscape Carbon Cycling: Research Needs for Resolving Organic Carbon Budgets of Lakes, Ecosystems, 18, 363–375, https://doi.org/10.1007/s10021-014-9826-9, 2015.

Hope, D., Palmer, S. M., Billett, M. F., and Dawson, J. J. C.: Variations in dissolved CO_2 and CH_4 in a first-order stream and catchment: an investigation of soil-stream linkages, Hydrol. Process., 18, 3255–3275, https://doi.org/10.1002/hyp.5657, 2004.

Jähne, B., Münnich, K. O., Bösinger, R., Dutzi, A., Huber, W., and Libner, P.: On the parameters influencing air-water gas exchange, J. Geophys. Res. Oceans, 92, 1937, https://doi.org/10.1029/JC092iC02p01937, 1987.

Jones, S. E., Kratz, T. K., Chiu, C.-Y., and McMahon, K. D.: Influence of typhoons on annual CO_2 flux from a subtropical, humic lake, Glob. Change Biol., 15, 243–254, https://doi.org/10.1111/j.1365-2486.2008.01723.x, 2009.

Kimura, N., Liu, W.-C., Chiu, C.-Y., and Kratz, T.: The influences of typhoon-induced mixing in a shallow lake, Lakes Reserv.: Res. Manag., 17, 171–183, https://doi.org/10.1111/j.1440-1770.2012.00509.x, 2012.

Kimura, N., Liu, W.-C., Tsai, J.-W., Chiu, C.-Y., Kratz, T. K., and Tai, A.: Contribution of extreme meteorological forcing to vertical mixing in a small, shallow subtropical lake, J. Limnol., 76, 116–128, https://doi.org/10.4081/jlimnol.2016.1477, 2017.

Kossin, J. P., Olander, T. L., and Knapp, K. R.: Trend Analysis with a New Global Record of Tropical Cyclone Intensity, J. Clim., 26, 9960–9976, https://doi.org/10.1175/JCLI-D-13-00262.1, 2013.

Kraemer, B. M., Pilla, R. M., Woolway, R. I., Anneville, O., Ban, S., Colom-Montero, W., Devlin, S. P., Dokulil, M. T., Gaiser, E. E., Hambright, K. D., Hessen, D. O., Higgins, S. N., Jöhnk, K. D., Keller, W., Knoll, L. B., Leavitt, P. R., Lepori, F., Luger, M. S., Maberly, S. C., Müller-Navarra, D. C., Paterson, A. M., Pierson, D. C., Richardson, D. C., Rogora, M., Rusak, J. A., Sadro, S., Salmaso, N., Schmid, M., Silow, E. A., Sommaruga, R., Stelzer, J. A. A., Straile, D., Thiery, W., Timofeyev, M. A., Verburg, P., Weyhenmeyer, G. A., and Adrian, R.: Climate change drives widespread shifts in lake thermal habitat, Nat. Clim. Chang., 11, 521–529, https://doi.org/10.1038/s41558-021-01060-3, 2021.

Lai, I.-L., Chang, S.-C., Lin, P.-H., Chou, C.-H., and Wu, J.-T.: Climatic Characteristics of the Subtropical Mountainous Cloud Forest at the Yuanyang Lake Long-Term Ecological Research Site, Taiwan, Taiwania, 51, 317–329, 2006.

Lauerwald, R., Laruelle, G. G., Hartmann, J., Ciais, P., and Regnier, P. A.: Spatial patterns in CO_2 evasion from the global river network, Global Biogeochem. Cycles, 29, 534–554, https://doi.org/10.1002/2014GB004941, 2015.

Lin, H.-C., Chiu, C.-Y., Tsai, J.-W., Liu, W.-C., Tada, K., and Nakayama, K.: Influence of Thermal Stratification on Seasonal Net Ecosystem Production and Dissolved Inorganic Carbon in a Shallow Subtropical Lake, J. Geophys. Res. Biogeosci., 126, https://doi.org/10.1029/2020JG005907, 2021.

Lin, H.-C., Tsai, J.-W., Tada, K., Matsumoto, H., Chiu, C.-Y., and Nakayama, K.: The impacts of the hydraulic retention effect and typhoon disturbance on the carbon flux in shallow subtropical mountain lakes, Sci. Total Environ, 803, 150044, https://doi.org/10.1016/j.scitotenv.2021.150044, 2022.

Maberly, S. C., O'Donnell, R. A., Woolway, R. I., Cutler, M. E. J., Gong, M., Jones, I. D., Merchant, C. J., Miller, C. A., Politi, E., Scott, E. M., Thackeray, S. J., and Tyler, A. N.: Global lake thermal regions shift under climate change, Nat Commun., 11, 1232, https://doi.org/10.1038/s41467-020-15108-z, 2020.

MacIntyre, S., Bastviken, D., Arneborg, L., Crowe, A. T., Karlsson, J., Andersson, A., Gålfalk, M., Rutgersson, A., Podgrajsek, E., and Melack, J. M.: Turbulence in a small boreal lake: Consequences for air-water gas exchange, Limnol. Oceanogr., 66, 827–854, https://doi.org/10.1002/lno.11645, 2021.

Maranger, R., Jones, S. E., and Cotner, J. B.: Stoichiometry of carbon, nitrogen, and phosphorus through the freshwater pipe, Limnol Oceanogr Lett, 3, 89–101, https://doi.org/10.1002/lol2.10080, 2018.

Marcé, R., Obrador, B., Gómez-Gener, L., Catalán, N., Koschorreck, M., Arce, M. I., Singer, G., and Schiller, D. von: Emissions from dry inland waters are a blind spot in the global carbon cycle, Earth-Sci. Rev., 188, 240–248, https://doi.org/10.1016/j.earscirev.2018.11.012, 2019.

Nagatomo, K., Nakayama, K., Komai, K., Matsumoto, H., Watanabe, K., Kubo, A., Tada, K., Maruya, Y., Yano, S., Tsai, J. W., Lin, H. C., Vilas, M., and Hipsey, M. R.: A Spatially Integrated Dissolved Inorganic Carbon (SiDIC) Model for Aquatic Ecosystems Considering Submerged Vegetation, J Geophys Res Biogeosci, 128, https://doi.org/10.1029/2022JG007032, 2023.

Nakayama, K., Kawahara, Y., Kurimoto, Y., Tada, K., Lin, H.-C., Hung, M.-C., Hsueh, M.-L., and Tsai, J.-W.: Effects of oyster aquaculture on carbon capture and removal in a tropical mangrove lagoon in southwestern Taiwan, Sci. Total Environ, 156460, https://doi.org/10.1016/j.scitotenv.2022.156460, 2022.

Nakayama, K., Komai, K., Tada, K., Lin, H. C., Yajima, H., Yano, S., Hipsey, M. R., and Tsai, J. W.: Modeling dissolved inorganic carbon considering submerged aquatic vegetation, Ecol. Model., 431, 109188, https://doi.org/10.1016/j.ecolmodel.2020.109188, 2020.

Nakayama, K., Sivapalan, M., Sato, C., and Furukawa, K.: Stochastic characterization of the onset of and recovery from hypoxia in Tokyo Bay, Japan: Derived distribution analysis based on “strong wind” events, Water Resour. Res., 46, https://doi.org/10.1029/2009WR008900, 2010.

Nash, J. E. and Sutcliffe, J. V.: River flow forecasting through conceptual models, I A discussion of principles, J. Hydrol., 10, 398–409, 1970.

Olsson, F., Mackay, E. B., Barker, P., Davies, S., Hall, R., Spears, B., Exley, G., Thackeray, S. J., and Jones, I. D.: Can reductions in water residence time be used to disrupt seasonal stratification and control internal loading in a eutrophic monomictic lake?, J. Environ. Manage., 304, 114169, https://doi.org/10.1016/j.jenvman.2021.114169, 2022a.

Olsson, F., Mackay, E. B., Moore, T., Barker, P., Davies, S., Hall, R., Spears, B., Wilkinson, J., and Jones, I. D.: Annual water residence time effects on thermal structure: A potential lake restoration measure?, J. Environ. Manage., 314, 115082, https://doi.org/10.1016/j.jenvman.2022.115082, 2022b.

Plummer, L. and Busenberg, E.: The solubilities of calcite, aragonite and vaterite in CO_2-H_2O solutions between 0 and 90°C, and an evaluation of the aqueous model for the system $CaCO_3$-CO_2-H_2O, Geochim. Cosmochim. Acta, 46, 1011–1040, https://doi.org/10.1016/0016-7037(82)90056-4, 1982.

Raymond, P. A., Hartmann, J., Lauerwald, R., Sobek, S., McDonald, C., Hoover, M., Butman, D., Striegl, R., Mayorga, E., Humborg, C., Kortelainen, P., Dürr, H., Meybeck, M., Ciais, P., and Guth, P.: Global carbon dioxide emissions from inland waters, Nature, 503, 355–359, https://doi.org/10.1038/nature12760, 2013.

Schindler, D. W., Curtis, P. J., Parker, B. R., and Stainton, M. P.: Consequences of climate warming and lake acidification for UV-B penetration in North American boreal lakes, Nature, 379, 705–708, https://doi.org/10.1038/379705a0, 1996.

Scully, N. M., McQueen, D. J., and Lean, D. R. S.: Hydrogen peroxide formation: The interaction of ultraviolet radiation and dissolved organic carbon in lake waters along a 43-75°N gradient, Limnol. Oceanogr., 41, 540–548, https://doi.org/10.4319/lo.1996.41.3.0540, 1996.

Shade, A., Chiu, C.-Y., and McMahon, K. D.: Seasonal and episodic lake mixing stimulate differential planktonic bacterial dynamics, Microb. Ecol., 59, 546–554, https://doi.org/10.1007/s00248-009-9589-6, 2010.

Shade, A., Read, J. S., Welkie, D. G., Kratz, T. K., Wu, C. H., and McMahon, K. D.: Resistance, resilience and recovery: aquatic bacterial dynamics after water column disturbance, Environ. Microbiol., 13, 2752–2767, https://doi.org/10.1111/j.1462-2920.2011.02546.x, 2011.

Shih, Y.-T., Chen, P.-H., Lee, L.-C., Liao, C.-S., Jien, S.-H., Shiah, F.-K., Lee, T.-Y., Hein, T., Zehetner, F., Chang, C.-T., and Huang, J.-C.: Dynamic responses of DOC and DIC transport to different flow regimes in a subtropical small mountainous river, Hydrol. Earth Syst. Sci., 22, 6579–6590, https://doi.org/10.5194/hess-22-6579-2018, 2019.

Smith, S. V.: Physical, chemical and biological characteristics* of CO_2 gas flux across the air-water interface, Plant Cell Environ., 8, 387–398, https://doi.org/10.1111/j.1365-3040.1985.tb01674.x, 1985.

Sobek, S., Tranvik, L. J., and Cole, J. J.: Temperature independence of carbon dioxide supersaturation in global lakes, Global Biogeochem. Cycles, 19, GB2003, https://doi.org/10.1029/2004GB002264, 2005.

Tranvik, L. J., Downing, J. A., Cotner, J. B., Loiselle, S. A., Striegl, R. G., Ballatore, T. J., Dillon, P., Finlay, K., Fortino, K., Knoll, L. B., Kortelainen, P. L., Kutser, T., Larsen, S., Laurion, I., Leech, D. M., McCallister, S. L., McKnight, D. M., Melack, J. M., Overholt, E., Porter, J. A., Prairie, Y., Renwick, W. H., Roland, F., Sherman, B. S., Schindler, D. W., Sobek, S., Tremblay, A., Vanni, M. J., Verschoor, A. M., Wachenfeldt, E. von, and Weyhenmeyer, G. A.: Lakes and reservoirs as regulators of carbon cycling and climate, Limnol. Oceanogr., 54, 2298–2314, https://doi.org/10.4319/lo.2009.54.6_part_2.2298, 2009.

Tsai, J.-W., Kratz, T. K., Hanson, P. C., Kimura, N., Liu, W.-C., Lin, F.-P., Chou, H.-M., Wu, J.-T., and Chiu, C.-Y.: Metabolic changes and the resistance and resilience of a subtropical heterotrophic lake to typhoon disturbance, Can. J. Fish. Aquat. Sci., 68, 768–780, https://doi.org/10.1139/F2011-024, 2011.

Tsai, J.-W., Kratz, T. K., Hanson, P. C., Wu, J.-T., Chang, W. Y. B., Arzberger, P. W., Lin, B.-S., Lin, F.-P., Chou, H.-M., and Chiu, C.-Y.: Seasonal dynamics, typhoons and the regulation of lake metabolism in a subtropical humic lake, Freshw. Biol., 53, 1929–1941, https://doi.org/10.1111/j.1365-2427.2008.02017.x, 2008.

Vachon, D. and Del Giorgio, P. A.: Whole-Lake CO_2 Dynamics in Response to Storm Events in Two Morphologically Different Lakes, Ecosystems, 17, 1338–1353, https://doi.org/10.1007/s10021-014-9799-8, 2014.

Vachon, D., Sponseller, R. A., and Karlsson, J.: Integrating carbon emission, accumulation and transport in inland waters to understand their role in the global carbon cycle, Glob. Change Biol., 27, 719–727, https://doi.org/10.1111/gcb.15448, 2021.

Walvoord, M. A. and Striegl, R. G.: Increased groundwater to stream discharge from permafrost thawing in the Yukon River basin: Potential impacts on lateral export of carbon and nitrogen, Geophys. Res. Lett., 34, https://doi.org/10.1029/2007GL030216, 2007.

Wanninkhof, R.: Relationship between wind speed and gas exchange over the ocean, J. Geophys. Res. Oceans, 97, 7373, https://doi.org/10.1029/92JC00188, 1992.

Williamson, C. E., Morris, D. P., Pace, M. L., and Olson, O. G.: Dissolved organic carbon and nutrients as regulators of lake ecosystems: Resurrection of a more integrated paradigm, Limnol. Oceanogr., 44, 795–803, https://doi.org/10.4319/lo.1999.44.3_part_2.0795, 1999.

Winslow, L. A., Read, J. S., Hansen, G. J. A., and Hanson, P. C.: Small lakes show muted climate change signal in deepwater temperatures, Geophys. Res. Lett., 42, 355–361, https://doi.org/10.1002/2014GL062325, 2015.

Woolway, R. I., Anderson, E. J., and Albergel, C.: Rapidly expanding lake heatwaves under climate change, Environ. Res. Lett., 16, 94013, https://doi.org/10.1088/1748-9326/ac1a3a, 2021a.

Woolway, R. I., Jennings, E., Shatwell, T., Golub, M., Pierson, D. C., and Maberly, S. C.: Lake heatwaves under climate change, Nature, 589, 402–407, https://doi.org/10.1038/s41586-020-03119-1, 2021b.

Woolway, R. I., Kraemer, B. M., Lenters, J. D., Merchant, C. J., O'Reilly, C. M., and Sharma, S.: Global lake responses to climate change, Nat. Rev. Earth Environ., 1, 388–403, https://doi.org/10.1038/s43017-020-0067-5, 2020.

Woolway, R. I., Simpson, J. H., Spiby, D., Feuchtmayr, H., Powell, B., and Maberly, S. C.: Physical and chemical impacts of a major storm on a temperate lake: a taste of things to come?, Climatic Change, 151, 333–347, https://doi.org/10.1007/s10584-018-2302-3, 2018.

Wu, J.-T., Chang, S.-C., Wang, Y.-S., and Hsu, M.-K.: Characteristics of the acidic environment of the Yuanyang Lake (Taiwan), Bot. Bull. Acad. Sin., 42, 17–22, 2001.

Zwart, J. A., Sebestyen, S. D., Solomon, C. T., and Jones, S. E.: The Influence of Hydrologic Residence Time on Lake Carbon Cycling Dynamics Following Extreme Precipitation Events, Ecosystems, 20, 1000–1014, https://doi.org/10.1007/s10021-016-0088-6, 2017.

Table 1. Comparison of Yuan-Yang Lake's rainfall and hydrological records in typhoon and non-typhoon years.

Records	Typhoon years	Non-typhoon years
Time period (year)	2015-2016	2017-2018
Total precipitation (mm)	6,332	3,795
Total typhoon rainfall (mm)	2,254	0
Average water depth (m ± SD)	4.54 ± 1.7	4.51 ± 1.5
Average river discharge (m^3 d^{-1})	3,717	2,943
Transparency (Secchi disc depth, m ± SD)	1.58 ± 0.45	1.38 ± 0.28

Table 2. Parameters of the two-layer conceptual model in Yuan-Yang Lake

	Parameters	Value	Unit
Measurements			
Q_{out}	Outflow discharge	Daily data	$m^3\ d^{-1}$
Q_{in}	Inflow discharge	Daily data	$m^3\ d^{-1}$
Q_U	Upper layer Discharge	Daily data	$m^3\ d^{-1}$
Q_L	Lower layer discharge	Daily data	$m^3\ d^{-1}$
DIC_R	River inflow DIC	Monthly data	mg-C L^{-1}
DIC_U	Upper layer DIC	Monthly data	mg-C L^{-1}
DIC_L	Lower layer DIC	Monthly data	mg-C L^{-1}
Chl_U	Upper layer Chl *a*	Monthly data	mg L^{-1}
Chl_L	Lower layer Chl *a*	Monthly data	mg L^{-1}
DOC_U	Upper layer DOC	Monthly data	mg-C L^{-1}
DOC_L	Lower layer DOC	Monthly data	mg-C L^{-1}
F_{CO2}	Carbon emission (equation 7)	Monthly data	mg-C $m^2\ d^{-1}$
Constants			
V_{total}	Total lake volume	53,544	m^3
V_U	Upper layer volume	45,456	m^3
V_L	Lower layer volume	8,808	m^3
A_s	Lake surface area	36,000	m^2
A_I	The interface area	7,264	m^2
A_B	The bottom of lake area	3,520	m^2
C_U	Coefficient of the unit uniform	1,000	L m^{-3}
Unknow Constants			
α_{PU}, α_{PL}	Coefficients of photosynthesis	Constant	d^{-1}
α_{MU}, α_{ML}	Coefficients of mineralization	Constant	d^{-1}
w_I	Coefficient of vertical transportation	Constant	d^{-1}
BF_{DIC}, BF_{DOC}	Sediment DIC and DOC emission	Constant	mg-C L^{-1}
Pa_U, Pb_L	Equations constant at lower layer	Constant	mg $m^{-3}\ d^{-1}$

Table 3. Best-fit parameters of a two-layer conceptual model of DIC and DOC in Yuan-Yang Lake from 2015 to 2018.

	2015–2016 Typhoon years				**2017–2018 Non-typhoon years**				**2015–2016 Typhoon years**	**2017–2018 Non-typhoon years**
	Spring	*Summer*	*Autumn*	*Winter*	*Spring*	*Summer*	*Autumn*	*Winter*	*Inter-annual*	*Inter-annual*
<u>*Upper layer*</u>										
F_{CO2} (mg-C m^2 d^{-1})	291	245	422	127	231	143	104	175	276	163
α_{PU} (d^{-1})	-1.20	-33.1	-183.5	-29.1	8.0	6.0	30.0	7.77	-22.0	8.0
α_{MU} (d^{-1})	-0.0227	0.0203	0.08	-0.031	-0.01	-0.039	-0.033	-0.195	-0.035	-0.0238
w_I (d^{-1})	0.230	0.172	1.38	0.30	0.10	0.0478	0.120	0.180	0.159	0.107
Pa_U (d^{-1})	12560	-1317	-23750	9597	9880	14000	17600	10100	4457	12420
Pb_U (d^{-1})	-21930	9461	-42130	-17070	-3630	-1251	-20820	-9289	-12760	-9119
$d\mathrm{DIC}_U$ (R^2, NSE)	0.305, 0.614								0.072, 0.299	0.403, 0.650
$d\mathrm{DOC}_U$ (R^2, NSE)	0.909, 0.953								0.242, 0.569	0.320, 0.918
<u>*Lower layer*</u>										
α_{PL} (d^{-1})	-0.627	-22.1	15.0	-0.878	1.49	-6.87	6.0	-16.6	-21.11	2.0
α_{ML} (d^{-1})	-0.025	0.123	0.0755	0.00973	-0.010	-0.0376	-0.04	-0.048	0.123	-0.019
Pa_L (d^{-1})	100	-5662	-10500	-1013	151.6	2032	1216	909	-5662	-40.5
Pb_L (d^{-1})	-6012	-7395	-53940	-9639	-1338	-6296	-19470	-8748	-12240	-9919
BF_{DIC}, BF_{DOC} (mg-C L^{-1})	0.04, 0.00									
$d\mathrm{DIC}_L$ (R^2, NSE)	0.452, 0.707								0.192, 0.306	0.440, 0.731
$d\mathrm{DOC}_L$ (R^2, NSE)	0.460, 0.728								0.234, 0.338	0.128, 0.525

Table 4. Seasonal averages of carbon fluxes (mg C m^{-3} d^{-1}) for each season in Yuan-Yang Lake. Positive values are shown in the carbon sink (*black*), and negative ones show the values after carbon was released (*red*).

		Flux (mg C m^{-3} d^{-1})			$\frac{DIC_U}{DOC_U}$	$\frac{DIC_L}{DOC_L}$	Total (mg C m^{-3} d^{-1})	
		F_C	**Upper**	**Lower**			$Flux_{DIC}$	$Flux_{DOC}$
Typhoon years	**Average**	**-219**	-	-	-	-	**-150**	**-9.69**
Spring	DIC	-231	-243	-45.2	0.658	0.568	-210	62.1
	DOC	-	70.8	17.2				
Summer	DIC	-194	29.1	-313	0.193	0.511	-26.4	18.8
	DOC	-	118	-495				
Autumn	DIC	-351	-216	-659	0.349	0.475	-288	-151
	DOC	-	46.1	-1167				
Winter	DIC	-100	-96.4	36.5	0.442	0.372	-74.8	31.2
	DOC	-	40.5	-16.9				
Non-typhoon years	**Average**	**-133**	-	-	-	-	**-47.8**	**52.6**
Spring	DIC	-129	-180	-94.9	0.524	0.634	-166	-7.06
	DOC	-	21.4	-67.1				
Summer	DIC	-183	5.80	-58.1	0.260	0.423	-4.57	73.8
	DOC	-	115	-140				
Autumn	DIC	-82.6	95.0	35.9	0.216	0.351	85.5	95.9
	DOC	-	168	-272				
Winter	DIC	-138	-128	6.04	0.449	0.436	-106	33.7
	DOC	-	34.0	32.1				

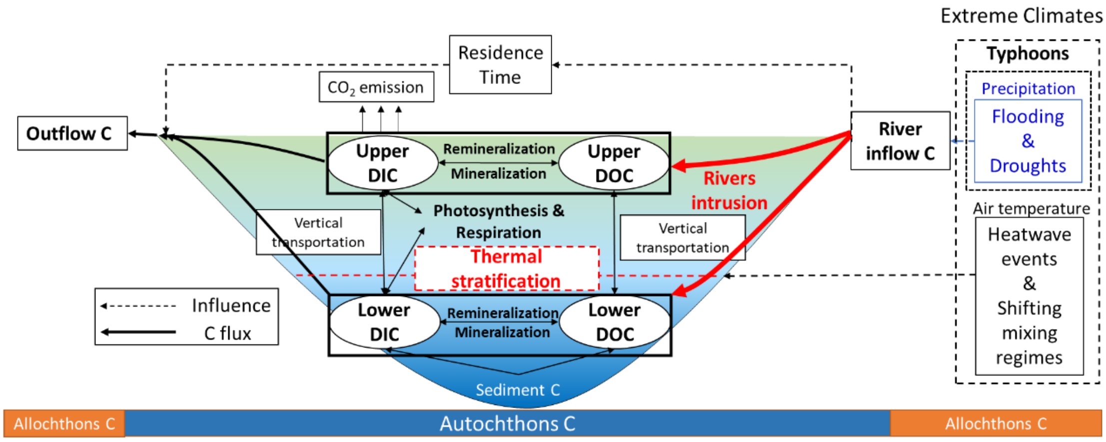

Fig. 1. Conceptual diagram of river intrusion (*red arrows*) and thermal stratification (*red dashed line*) dominant responses of DIC and DOC in a subtropical two-layer stratified lake under extreme climates.

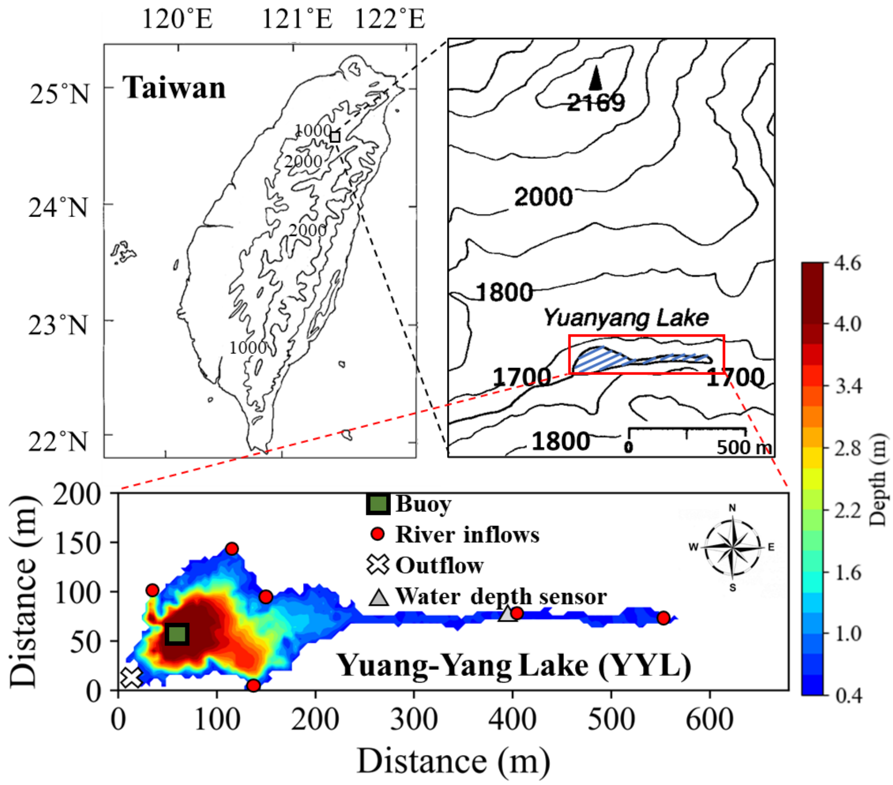

Fig. 2. Sampling locations and bathymetry maps of Yuan–Yang Lake (YYL). The dark green rectangle shows the buoy station, which is at the deepest site of the lake. The red points and white cross show the river mouths of the inflows and outflows, respectively. The gray triangle shows the location of the water depth sensor.

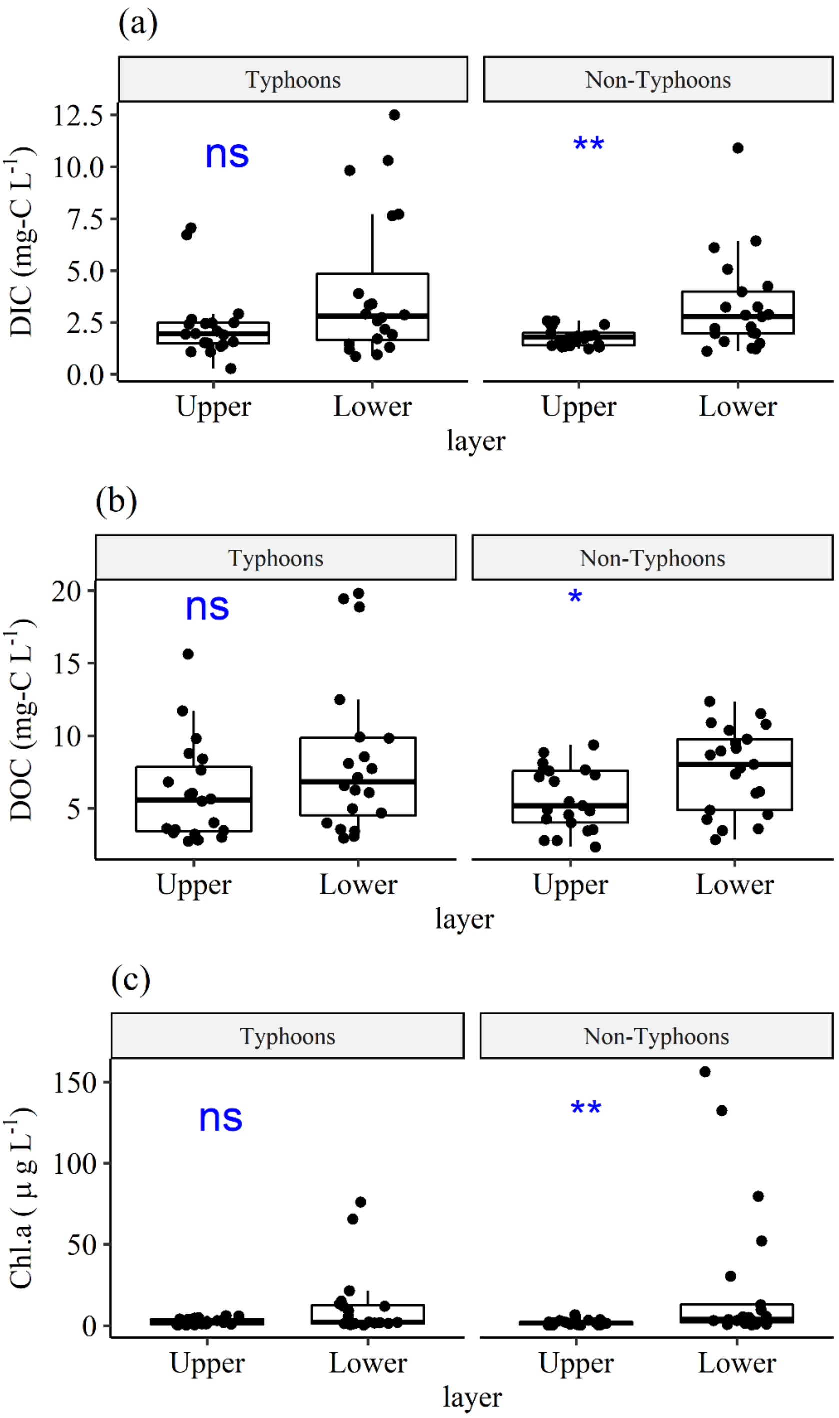

Fig. 3. Comparisons of **(a)** DIC, **(b)** DOC, and **(c)** Chl *a* between upper (DIC_U, DOC_U, Chl_U) and lower (DIC_L, DOC_L, Chl_L) layers, grouped by typhoon and non-typhoon years. The bullet points show the water sampling data. We used a t-test to obtain the *p*-values. The **ns** show the *p*-values ≥ 0.05, * show *p*-values from 0.05 to 0.01, and ** show p-values from 0.01 to 0.001 by t-test.

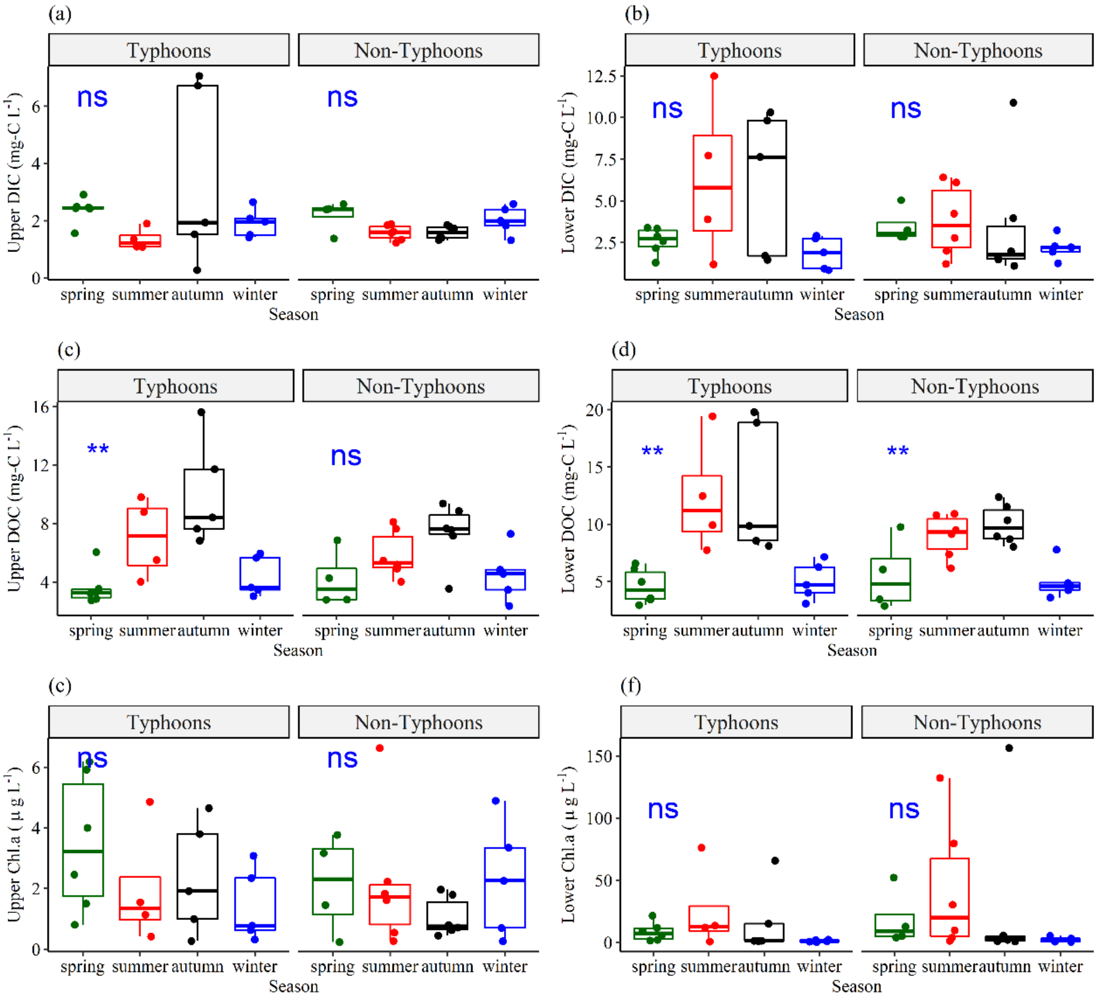

Fig. 4. Seasonal variations of **(a)** upper layer DIC (DIC_U), **(b)** lower layer DIC (DIC_L), **(c)** upper layer DOC (DOC_U), **(d)** lower layer DOC (DOC_L), **(e)** upper layer Chl. a (Chl_U), **(f)** lower layer Chl. *a* (Chl_L) grouped by typhoon and non-typhoon years. The bullet points show the water sampling data. To determine the seasonality, we used one-way ANOVA to obtain the *p*-values. The **ns** show p-values ≥ 0.05, * show *p*-values from 0.05 to 0.01, and ** show *p*-values are from 0.01 to 0.001.

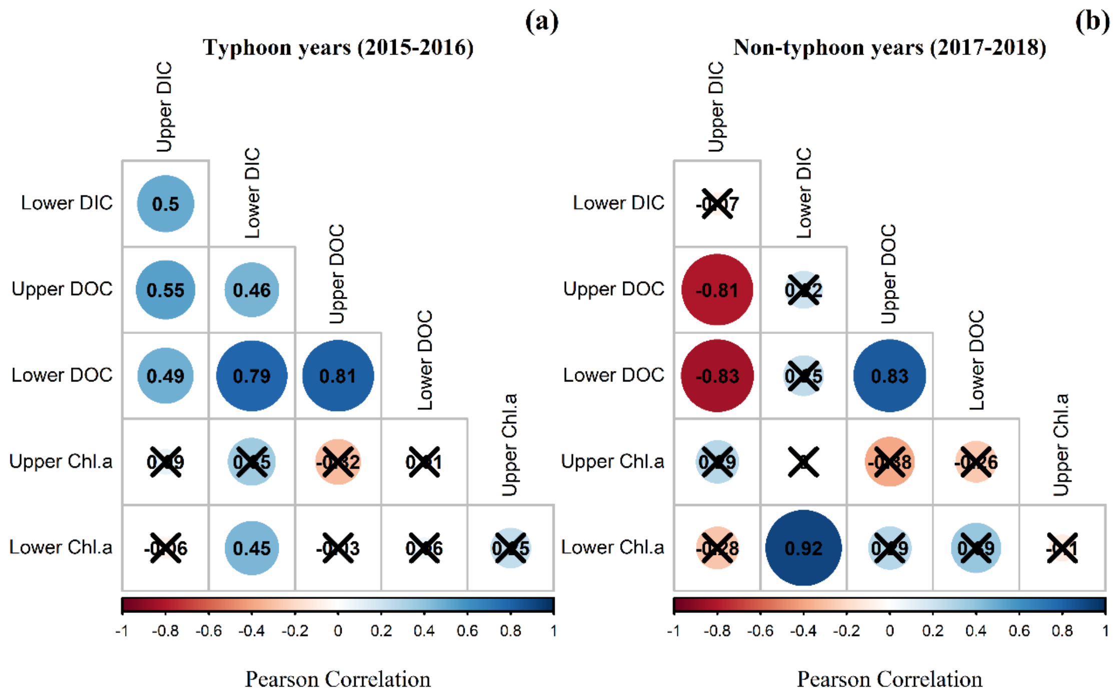

Fig. 5. Pearson correlation coefficients of DIC, DOC, and Chl. *a* concentration at upper layer and lower layer DIC ($DIC_U,\ DIC_L$), DOC ($DOC_U,\ DOC_L$), Chl. a ($Chl_U,\ Chl_L$) during **(a)** typhoon years and **(b)** non-typhoon years. The *black-crosses* show insignificant values (*p*-values are > 0.05).

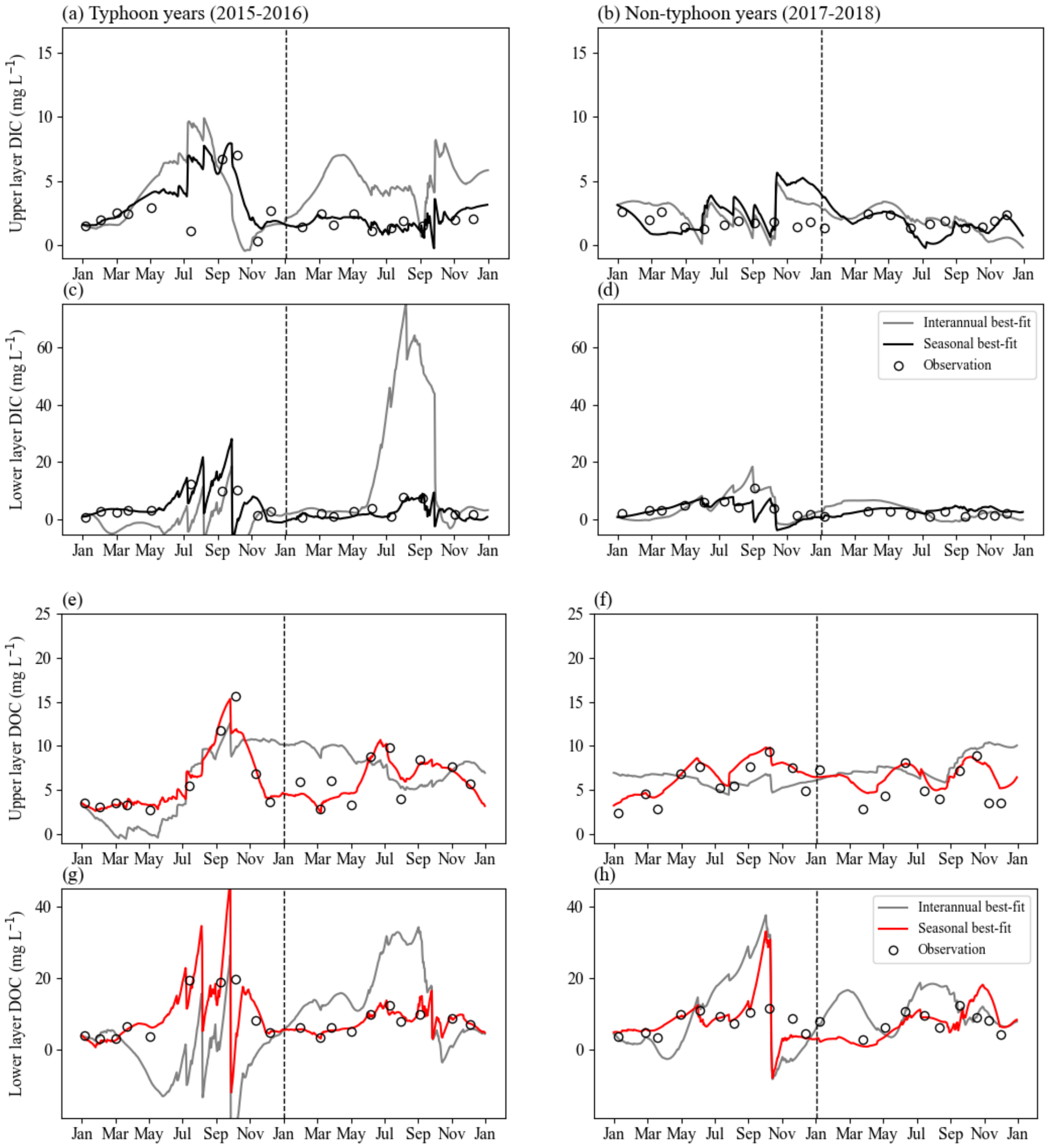

Fig. 6. Continuous daily DIC and DOC data at **(a, b, e, f)** the upper layer (DIC_U, DOC_U) and **(c, d, g, h)** lower layer (DIC_L, DOC_L) by using conceptual equations models. The *gray lines* show the interannual data, the *black lines* show the *best fit* for DIC, the *red lines* show the *best-fit* for DOC (**Table 3**), and the *empty dots* show water sampling (observation) data for each month.

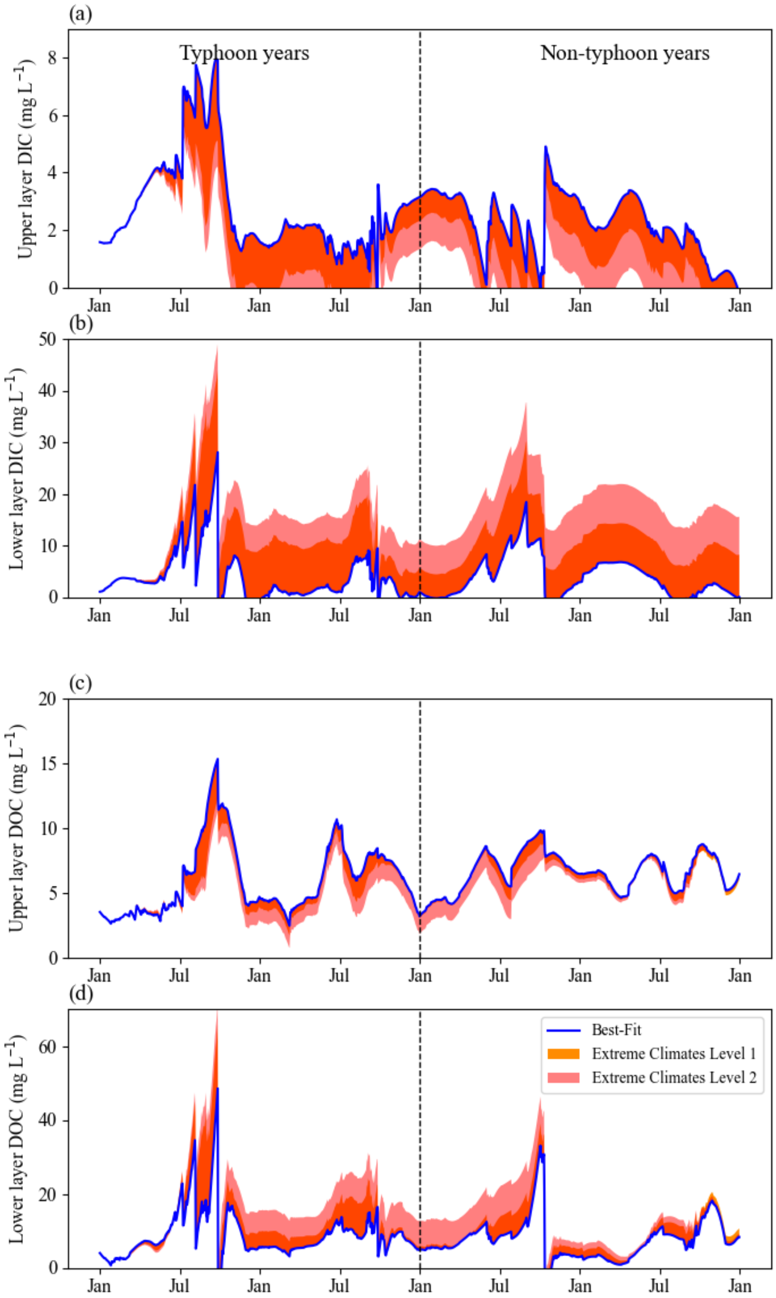

Fig. 7. Continuous daily DIC and DOC data at **(a, c)** upper layer (DIC_U, DOC_U) and **(b, d)** lower layer (DIC_L, DOC_L) by using the conceptual equation model under extreme climates from 2015 to 2018. *Blue lines* are original best-fit data as in Fig. 6, in which the parameters of the DIC model in non-typhoon years are under the nonseasonal scenario and the others are under the seasonal scenario as in Table 3. *Orange regions* show *Level 1*; *pink regions* show *Level 2*.

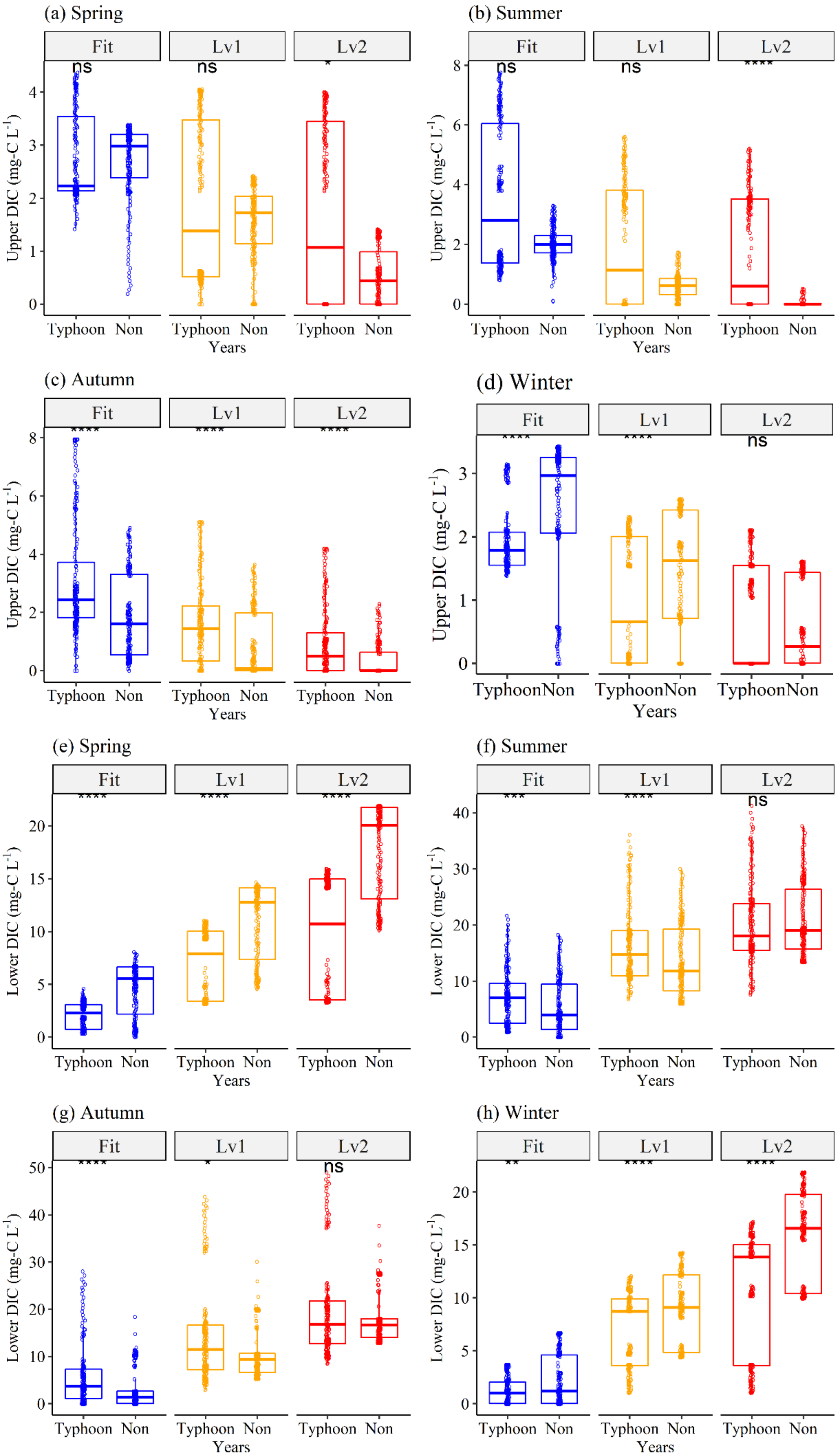

(a) Spring
(b) Summer
(c) Autumn
(d) Winter
(e) Spring
(f) Summer
(g) Autumn
(h) Winter
Fit
Lv1
Lv2
Upper DIC (mg-C L-1)
Lower DIC (mg-C L-1)
Typhoon
Non
Years
ns

751

Figure 8. Seasonal responses of continuous **(a-d)** upper layer DIC and **(e-h)** lower layer DIC (mg-C L^{-1}) between typhoon (*Typhoon*) and non-typhoon (*Non*) years for each season as in **Fig. 4**. *Fit* (*blue boxes*) condition shows the best-fit data by using the conceptual two-layer C model; *Lv1* (*yellow boxes*) and *Lv2* (*red boxes*) show the extreme climates. The empty dots show the continuous DIC and DOC data. The **ns** show p-values ≥ 0.05, * show p-values from 0.05 to 0.01, ** show p-values from 0.01 to 0.001; **** show p-values less than 0.0001 based on a t-test.

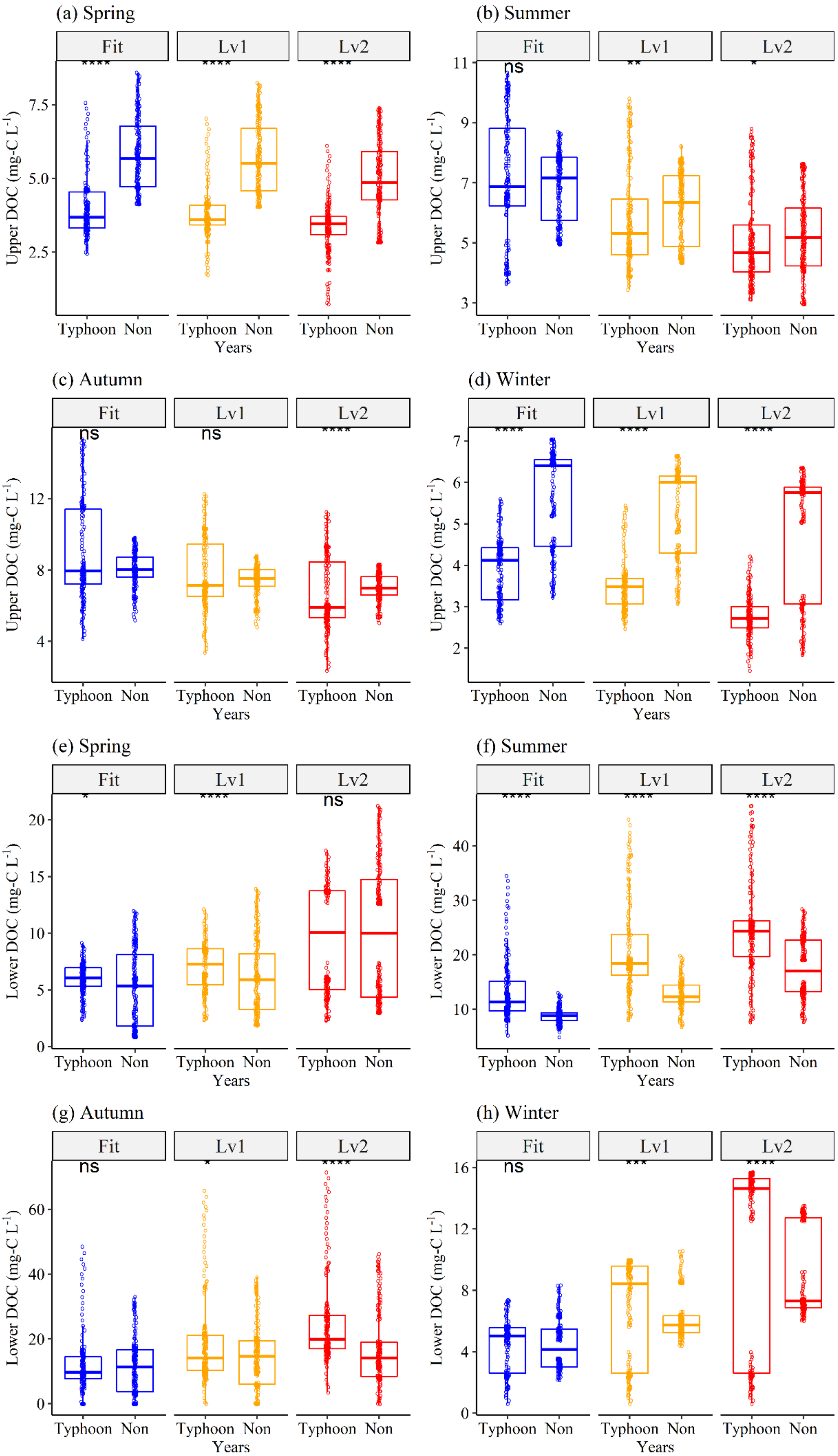
(a) Spring
(b) Summer
(c) Autumn
(d) Winter
(e) Spring
(f) Summer
(g) Autumn
(h) Winter
Fit
Lv1
Lv2
****
**
***
*
ns
Upper DOC (mg-C L-1)
Lower DOC (mg-C L-1)
Typhoon
Non
Years

Fig. 9. Seasonal responses of **(a-d)** upper layer DOC and **(e-h)** lower layer DOC (mg-C L^{-1}) between typhoon (*Typhoon*) and non-typhoon (*Non*) years for each season as in Fig. 8. The *Fit* (*blue boxes*) condition shows the best-fit data by using the conceptual two-layer carbon model; *Lv1* (*yellow boxes*) and *Lv2* (*red boxes*) show the extreme climates. Empty dots show the continuous DIC and DOC data. The **ns** show p-values ≥ 0.05, ***** show p-values from 0.05 to 0.01, ****** show p-values from 0.01 to 0.001; ******** show p-values less than 0.0001 based on a t-test.

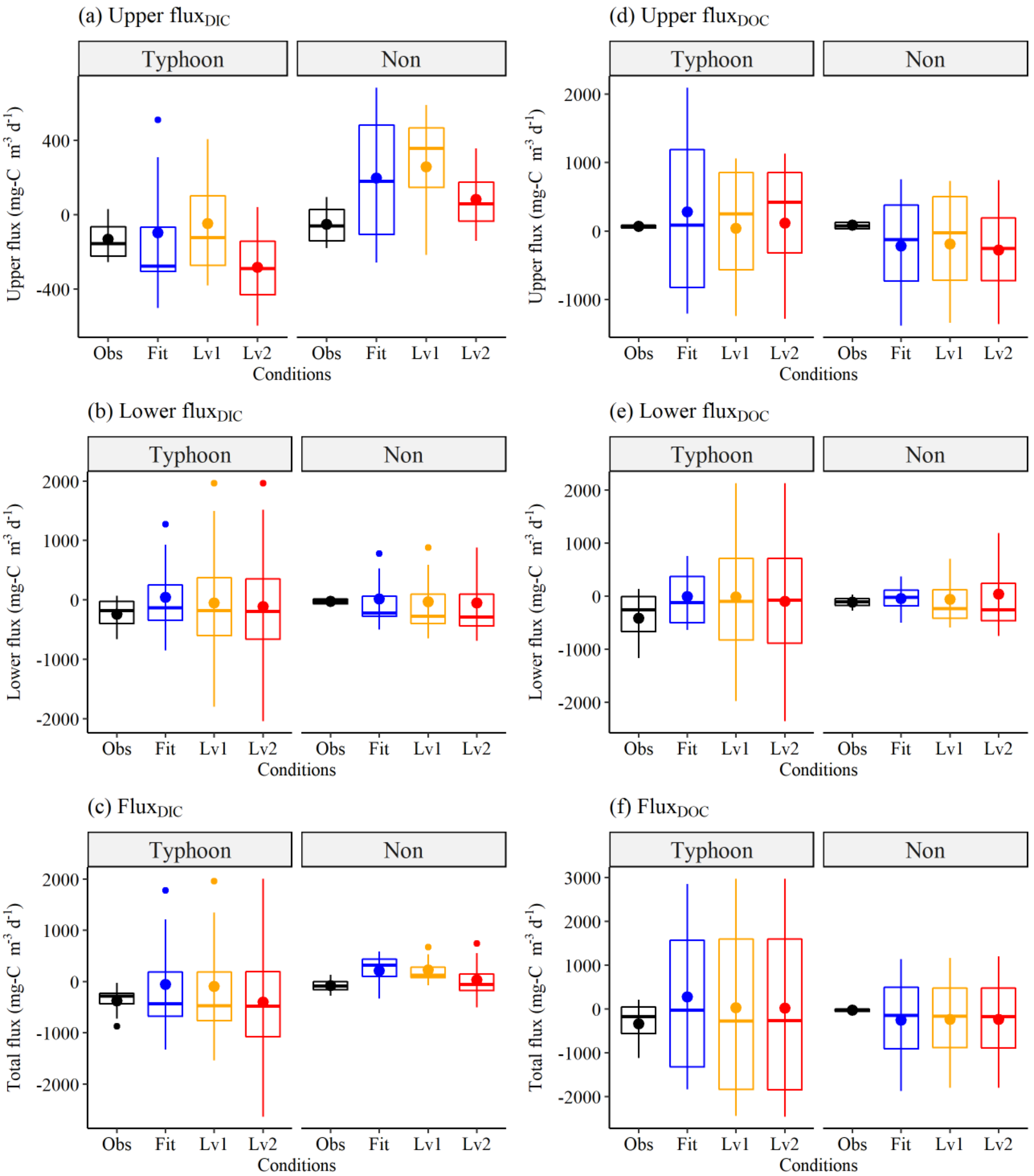

Fig. 10. Interannual (a) Upper flux$_{DIC}$, (b) Lower flux$_{DIC}$, (c) Flux$_{DIC}$, (d) Upper flux$_{DOC}$, (e) Lower flux$_{DOC}$, and (f) Flux$_{DOC}$ (mg C m^{-3} d^{-1}) grouped by typhoon and non-typhoon years. The *Obs* condition (*black boxes*) show the observation data as in Fig. 6; The *Fit* condition (*blue- boxes*) shows the best-fit data by using the conceptual two-layer carbon model as in Fig.6; *Level 1* (*yellow boxes*) and *Level 2* (*red boxes*) show the extreme scenarios as in Fig. 7. The definitions of fluxes please see Sect. 2.3.3.